Title

Study of signal transduction in reconstituted membranes: Ras activation by SOS and RasGRP1

Author

Tu, Hsiung-Lin

Publication Date

2013

Study of signal transduction in reconstituted membranes: Ras activation by SOS and RasGRP1

By

Hsiung-Lin Tu

A dissertation submitted in partial satisfaction of the
requirements for the degree of
Doctor of Philosophy
in
Chemistry
in the
Graduate Division
of the
University of California, Berkeley

Committee in charge:
Professor Jay T. Groves, Chair
Professor John Kuriyan
Professor Kunxin Luo
Spring 2013

Study of signal transduction in reconstituted membranes:
Ras activation by SOS and RasGRP1

By

Hsiung-Lin Tu

Abstract

Study of signal transduction in reconstituted membranes: Ras activation by SOS and RasGRP1

by

Hsiung-Lin Tu

Doctor of Philosophy in Chemistry

University of California, Berkeley

Professor Jay T. Groves, Chair

Cellular membranes organize signal transduction, serving as platforms for protein interactions, as well as direct modulators of enzyme function. Since many signaling reactions converge at the plasma membrane, understanding the coupling between protein function and membrane localization of signaling complex is of fundamental importance. However, a quantitative description of many of such interactions has been lacking, largely due to the difficulty in performing measurements in the complex cellular environment. Here, we reconstitute and quantitatively probe the kinetics between small GTPase Ras and its activators: Son of Sevenless (SOS) and Ras guanyl nucleotide-releasing protein (RasGRP) using supported membranes.

The activation of the membrane-associated Ras by cytosolic guanine nucleotide exchange factors, SOS and RasGRP, is a key step in a plethora of receptor-mediated cell signaling pathways. Both SOS and RasGRP contain multiple domains and several of which are known to regulate the activation of SOS/RasGRP. In this dissertation, we study in parallel the kinetics of SOS and RasGRP-catalyzed Ras activation as well as the mechanisms that release the autoinhibition of SOS/RasGRP at single molecule level.

We develop an assay with supported bilayers functionalized with H-Ras to monitor the enzymatic activities from hundreds of individual SOS proteins. The data reveals that SOS is dynamically heterogeneous, sampling a broad distribution of turnover rates via stochastic fluctuations between distinct states. The regulatory domains allosterically inhibit SOS by suppressing fluctuations to high activity states with sensitivity to both Ras nucleotide state and lipids. On the subject of Ras activation by RasGRP, the functional role of lipid interacting C1 domain of RasGRP1 has been studied. The preliminary results suggest that diacylglycerol (DAG), through the interaction with the C1 domain, regulates the function of RasGRP1 primarily by increasing its membrane localization.

To my beloved family & Jui-Lun

Table of Contents

List of Figures

Acknowledgement

I would like to thank many people. My advisor, Prof. Jay T. Groves, for his continuous support and great scientific insights. The Groves lab has been a great working environment and I truly enjoy and appreciate all the help I have ever received. I would like to thank Dr. Lars Iversen, Dr. Wan-Chen Lin and Dr. Sune Christensen (RasSOS team ☺), with whom I worked closely in various projects, for their not only scientific mentoring but also teach me how to find good work-life balance over the years.

I would also like to thank many collaborators, Prof. John Kuriyan and his lab members Dr. Jeff Iwig and Dr. Jodi Gureasko; Prof. Arthur Weiss; Prof. Arup Chakraborty and Dr. Steven Abel; Prof. Jeroen Roose and Dr. Jesse Jun, for their insightful knowledge and various supports in the projects. I would also thank Dr. Hung-Jen Wu, Dr. Rebecca Petit and Dr. Christopher Rhodes for their help and discussion at various stages of the projects. I would like to thank all the Groves lab members, for being so friendly and good colleagues.

Life is a continuous process. I would thank people who has helped and made my Berkeley experience possible. Prof. Chung-Yuan Mou, Prof. Peilin Chen, Prof. Fu-Yu Tsai and Dr. Yann Hung, for their help and mentoring in NTU and Academia Sinica, Taiwan.

I thank my parents for their 100% support and encourage me to pursue my dream; my brother and his family, for allowing me to focus on my graduate study knowing my parents will be taken good care of; Jui-Lun and her family for understanding and continuous support.

I also thank all friends and people I met in Berkeley. You all made my life. Cheers !!

Chapter 1 Introduction

The plasma membrane forms the physical boundary that defines intracellular space and outside environment. But more than a standstill barrier, there are many active processes such as the transport of small molecules and reorganization of proteins and lipids that are continuously taking place across/on the membrane (*1*). Indeed, one particularly interesting physical feature of cellular membrane, as a result of its complex constituents (lipids, sugars and proteins), is that the plasma membrane is highly dynamic both temporally and spatially which allows cells to respond quickly to changes in the surrounding environment (*1, 2*). At the intracellular level, such cellular response usually involves a chain of chemical reactions known as signal transduction. Signaling cascades are initiated from the membrane and relayed via a series of intracellular protein-protein as well as protein-lipid interactions, allowing physical processes such as membrane localization or chemical modifications such as protein phosphorylation to take place. Among many other interesting topics in membrane research, one involves the quest to understand the molecular mechanism of signal transduction, specifically how proteins are regulated and eventually get activated by means of recruitment to the vicinity of the signaling entity of interest and exert their functions (*3*).

Peripheral membrane proteins describe a class of proteins that is composed of one or more lipid interacting domains (*4*). One characteristic of these domains is their binding affinity towards specific lipids. For example, pleckstrin homology (PH) domain has been shown to specifically recognize phosphoinositide lipids whereas the C1 domain binds diacylglycerol (DAG) with high affinity (*4, 5*). The biological significance of these domains is to drive, in response to upstream signals, functionally important membrane recruitment of their "host" proteins to the correct spatial location. Without specific recognition provided by the binding domains, the "host" protein has very low chance to encounter its target proteins/molecules otherwise. In other words, the lipid-binding domains greatly enhance signaling specificity and fidelity. Additionally, after co-localization at the membrane, it has been shown that reaction kinetics can increase significantly, assuming both proteins in an interacting pair are localized to the surface, due to higher effective concentration of proteins (*3, 6*).

Although the individual functions of specific domains are relatively well understood, it is unclear how does a multi-domain protein with binding and catalytic domains integrate various inputs and act cooperatively in mediating complex biological processes (*4, 7*). Part of the reason is the lack of proper experimental platforms where the effect of individual components can be fine-tuned and tested quantitatively, eventually allowing one to dissect the underlying mechanism.

My dissertation has focused on developing the supported membrane technology to study signal transduction reactions. Specifically I have focused on understanding Ras activation by Son of Sevenless (SOS) and Ras guanyl nucleotide-releasing protein (RasGRP). In following chapter, a brief background for Ras signaling, SOS and RasGRP activation, and the supported bilayer platform will be introduced.

Chapter 2 Background

2.1 Ras signaling

Ras, first discovered more than three decades ago, is a founding member of small guanosine triphosphatases (GTPase) superfamily protein that now includes ~150 human proteins (*8*). All small GTPases bind to guanosine triphosphate (GTP) and guanosine diphosphate (GDP) in the lower nano-molar to pico-molar range and function as GDP/GTP regulated molecular switches (*9*). Another common feature among majority of Ras superfamily is their membrane association and subcellular localization through post-translational modification (PTM) by lipids. It is thus evident that physical recruitment is a common theme for other proteins (upstream, downstream, and effector) to exert their functions on small GTPases.

Following activation by plasma membrane receptors, Ras protein recruits and facilitates activation of a wide range of downstream effectors, regulating critical cellular processes such as cellular proliferation, differentiation and survival (*10*). Accordingly, Ras activation is tightly regulated in the cell, and its deregulation is a hallmark of many cancers and developmental defects. There are four Ras isoforms (H-Ras, N-Ras, K-Ras4A and K-Ras4B) that are ubiquitously expressed and share more than 90% sequence identity, especially in the G-domain (1-166 amino acids) where nucleotides are held in place by the switch I and II motifs. The four isoforms are not functionally redundant due to the differences in the C-terminal hypervariable region (HVR) and lipid modifications (Fig. 2-1). It has been shown that different lipid modifications direct Ras GTPases to unique subcellular compartments. For example, after PTM, K-Ras4B has been shown to mainly associate with plasma membrane whereas H-Ras and N-Ras localizes to both plasma membrane and Golgi membranes. The compartmentalized distribution of Ras isoforms is proposed to enable more spatially specific Ras signaling outputs within cells (*11*).

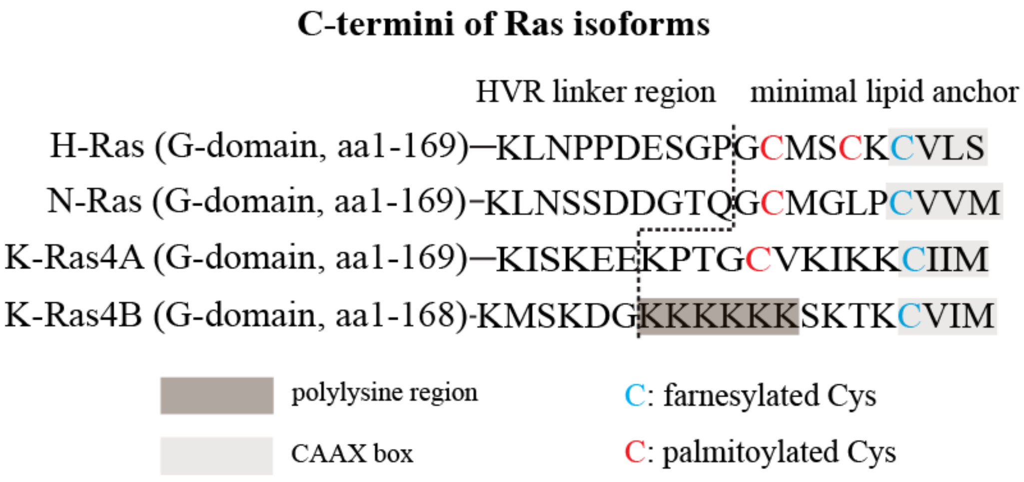

Figure 2-1. The hypervariable region and lipid modifications of Ras isoforms.

The importance of Ras signaling can be further realized provided there are several conditional PTMs such as peptidyl-prolyl isomerization, ubiquitylation and acetylation involved in maintaining normal level of Ras signaling (*12*). In fact, it has been shown that oncogenic Ras mutations occur in ~ 30% human cancers (*13*). As a consequence, Ras is a popular drug candidate for cancer treatment. Despite numerous attempts over the past two decades to inhibit or modulate Ras function with small molecules, the efficacy of the drugs remains poor (*12, 14*).

2.2 Ras regulation by GEF and GAP

Ras signaling is regulated primarily by switching its guanine nucleotide binding partner. Ras initiates downstream signaling only when binding to GTP (ON state). Without upstream stimuli, Ras is bound with GDP and cannot relay any signal (OFF state). Intrinsically, Ras slowly hydrolyzes (4.2 x 10-4 s^{-1}) bound GTP to GDP and enters OFF state (and hence the name GTPase) (*15, 16*). Conversely, activation of Ras involves the slow replacement of GDP by a GTP molecule in the nucleotide binding pocket (3.4 x 10-4 s^{-1}). Consequently, GDP/GTP exchange is catalyzed by proteins known as guanosine nucleotide exchange factors (GEFs) and GTPase-activating proteins (GAPs), respectively.

GEFs are proteins responsible for turning on small GTPases-mediated signaling by catalyzing the exchange of GDP to GTP that bound to GTPases. A general exchange mechanism involves the fast association of GEF to GDP-bound Ras to form a tertiary complex, which later converts into a high-affinity nucleotide-free Ras/GEF complex after dissociation of GDP. The latter step is found to be the rate-limiting step (*9*). Eventually, binding of GTP to Ras/GEF complex displaces GEF and yields the active form of the Ras (Ras-GTP). Surprisingly, the Ras/GEF complex does not favor the formation of the active GTP-bound complex. The resulting increase in GTP-bound over GDP-bound Ras, after GEF-mediated exchange, is due to the higher cellular concentration of GTP (~ 10 times greater than GDP) (*9, 17*).

The GAP proteins, on the other hand, are responsible for turning off Ras signaling and can be thought of as the more passive half of Ras regulation. Structural studies have provided great deal in understanding GAP catalyzed GTP hydrolysis and few key residues such as G12, G13 and Q61 of Ras that are involved in stabilizing the Ras/GTP/GAP intermediate during hydrolysis have been identified (*17, 18*). As mentioned above, the catalysis of Ras hydrolysis is very important, since the intrinsic hydrolysis rate of GTP is very slow, so GAPs provide an important function by continuously deactivating GTP bound Ras and hence terminating the downstream signaling.

GEFs and GAPs have in common that they are usually multi-domain proteins (*17*). Many of these domains are protein or lipid interacting domains, suggesting their role in serving as localization signals or as scaffolds for the formation of protein complexes (*17*). In fact, one of current focus in GEFs and GAPs research field is to understand how GEFs/GAPs are themselves being regulated and activated on the membrane surface (*19*). For example, a kinetic study on Arno, a GEF for small GTPase Arf involved in membrane traffic, indicated that PH domain of Arno not only binds to phosphoinositide but also interacts with an activating Arf family member on the liposome membrane (*20, 21*). This in turn allows Sec7, the catalytic unit of Arf, to activate more Arf on the membrane surface and thus a positive feedback loop was established (*20*).

2.3 SOS and coincidence detector

SOS is a GEF for Ras and the interaction between SOS and Ras has been the subject of a great deal of research. The canonical model of Ras activation by SOS, in response to upstream signals such as the activation of receptor tyrosine kinase, involves the recruitment of SOS to the plasma membrane via the adaptor protein Grb2. Membrane localization of SOS results in interaction with Ras and its consequent conversion from the inactive GDP- to the active GTP-bound state.

Later it was suggested that the aforementioned canonical model is far too simplistic. This is partly due to the better understanding of the structural aspects of SOS. Indeed, the molecular structure and domain organization of SOS has been determined and studied extensively over the years (*22-27*). From N- to C-terminal, SOS is comprised of a histone fold-like (HF), Dbl homology (DH), PH, Ras exchanger motif (REM), Cdc25 and Grb2 binding domains (Fig. 2-2). Several important features such as the existence of two Ras binding sites (*24*) and the multiple layers of autoinhibition imposed by the intra-molecular domain interactions have been described (*25, 27*). Later it was also established that a positive feedback loop associated with SOS mediated Ras activation is necessary for digital

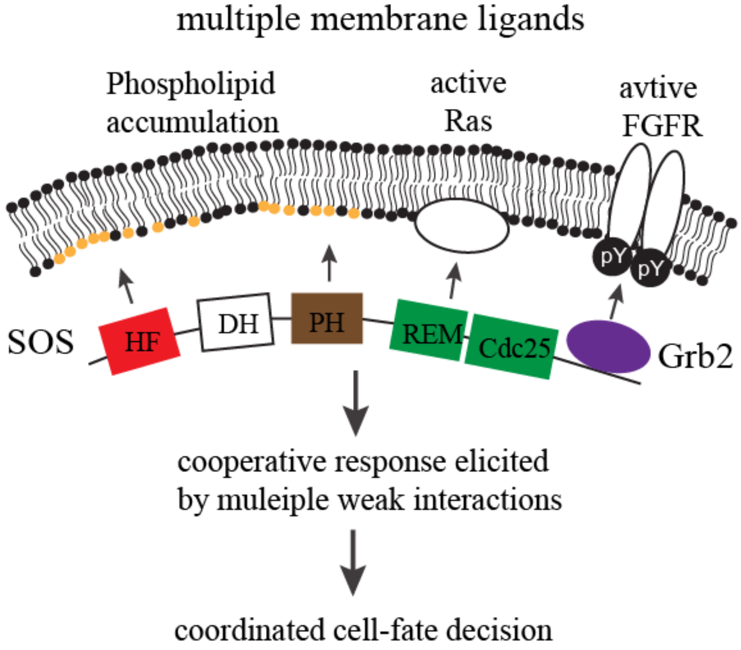

Figure 2-2. The proposed model of SOS activation. SOS is a multi-domain protein that interacts with various membrane ligands. A cooperative binding is required to fully activate SOS. The figure is modified based on [29].

signaling output, which has been suggested to play important role in the positive and negative selection in thymocytes (*28*).

A recent work on embryonic stem cells by Findlay and colleagues pointed out that the "balanced" interaction between the domains of SOS/Grb2 to their membrane substrates (Ras and phospholipids) is important in the regulation of pluripotency and differentiation factors during mammalian development (*29*). Based on numerous structural and cell studies, the emerging model for Ras activation by SOS suggested that SOS acts as a coincidence detector, which is fully activated only when it recognizes all the cognate ligands (Fig. 2-2) and thus confers signaling fidelity.

An important feature of coincidence detection is the binding affinity of individual module is usually rather weak, thereby allowing the protein to disengage if necessary and continue to search for its target(s) (*30*). In fact, a genome-wide analysis of 33 yeast PH domains showed that, of those that bind phosphoinositides, most did so weakly and promiscuously, yet still got recruited in a phosphoinositides-dependent manner (*31*). The idea of coincidence detector has also been demonstrated in other signaling systems. For example, full activation of WAVE2 complex, which is involved in actin nucleation, requires simultaneous signals from (1) prenylated activated Rac (Rac-GTP), (2) acidic phospholipids, and (3) the phosphorylation of WAVE2 complex (*32*). Similarly, it has been shown that binding to DAG, negatively charged lipids and Ca^{2+} ions through C1 and C2 domain of protein kinase C (PKC) are required to fully activate PKC at the membrane (*33*).

2-4 Ras activation via RasGRP

Ras guanyl nucleotide-releasing protein (RasGRP) represents another family of GEFs for Ras activation. Four members including RasGRP1, RasGRP2, RasGRP3 and RasGRP4 were identified (*34*). All RasGRP contains REM and Cdc25 domains that are required to mediate nucleotide exchange and activate Ras. Distinct structural features that distinguish RasGRP from other RasGEF is a pair of EF-hands and a C1 domain located C-terminal to the REM and Cdc25 domains (*35*). The C1 domain is a cysteine-rich domain containing ~50 residues. First identified in PKC, the C1 domain is known to bind to the lipid second messenger diacylglycerol (DAG) (*36, 37*). DAG is generated at the membrane by a variety of receptors, therefore, binding of C1 domain to DAG can serve as a DAG-dependent Ras activation pathway. In fact, it was later found that RasGRP1 becomes activated and triggered Ras signaling in response to TCR signaling in a PLC- and DAG-dependent fashion in the Jurkat T cell line (*38*).

2-5 Supported Lipid Bilayers

Supported lipid bilayers (SLBs) has been widely used as a model system to study protein-protein and protein-cell interactions on the surface (*39, 40*). It is composed of lipid molecules that diffuse laterally with diffusion coefficients generally on the order of 1 um^2/s on a solid support such as silicon oxide (*41*). The two dimensional fluidity is essential to mimic the natural cell membrane in order to study protein-protein interaction in its native membrane environment and the importance to preserve such physical property has been highlighted and demonstrated in various systems (*3, 6, 26*).

Figure 2-3 illustrates a general procedure to prepare the SLBs on a hydrophilic glass surface. First, one needs to decide the lipid composition. Two most important considerations are the types of lipids (ex: charge state) and the coupling chemistry (for a more detail discussion, please see (*39*)). After mixing the lipids in organic solvent, a dried lipid film is spontaneous formed once solvent is removed by rotary evaporation. In the meantime, small unilamellar vesicle (SUV) containing lipids of interest is prepared by extruding the hydrated lipid vesicles (Fig. 2-3(A)). SUVs is then added to the cleaned, hydrophilic glass surface and allowed to fuse spontaneously and form the SLBs (*39*) (Fig. 2-3(B) and (C)). Excess, unfused SUVs are then removed from the system by extensive wash with buffer. Now, the protein of interest can be functionalized onto the bilayer through proper chemical linkage. In this dissertation, the maleimide-cysteine chemistry is used, specifically cysteine at position 181 of H-Ras is chemically linked to the maleimide group of a functional lipid (MCC-DOPE) (Fig. 2-3(D)) (*26*).

In general, SLBs offers the following advantages to study signaling reaction on the membrane: (1) the lipid composition and surface density of protein can be easily controlled and manipulated; (2) planar geometry of the solid support allows the use of wide ranges of microscopic and spectroscopic techniques to perform measurements; (3) the availability of a selection of functional lipids enables the protein functionalization to take place via several coupling strategies such as maleimide-cysteine, Nickel-nitrilotriacetic acid (Ni-NTA), DNA hybridization and etc (*39*); (4) the compatibility of supported membrane with other surface fabrication techniques makes it possible to perform experiments with desired spatial resolution (*42, 43*).

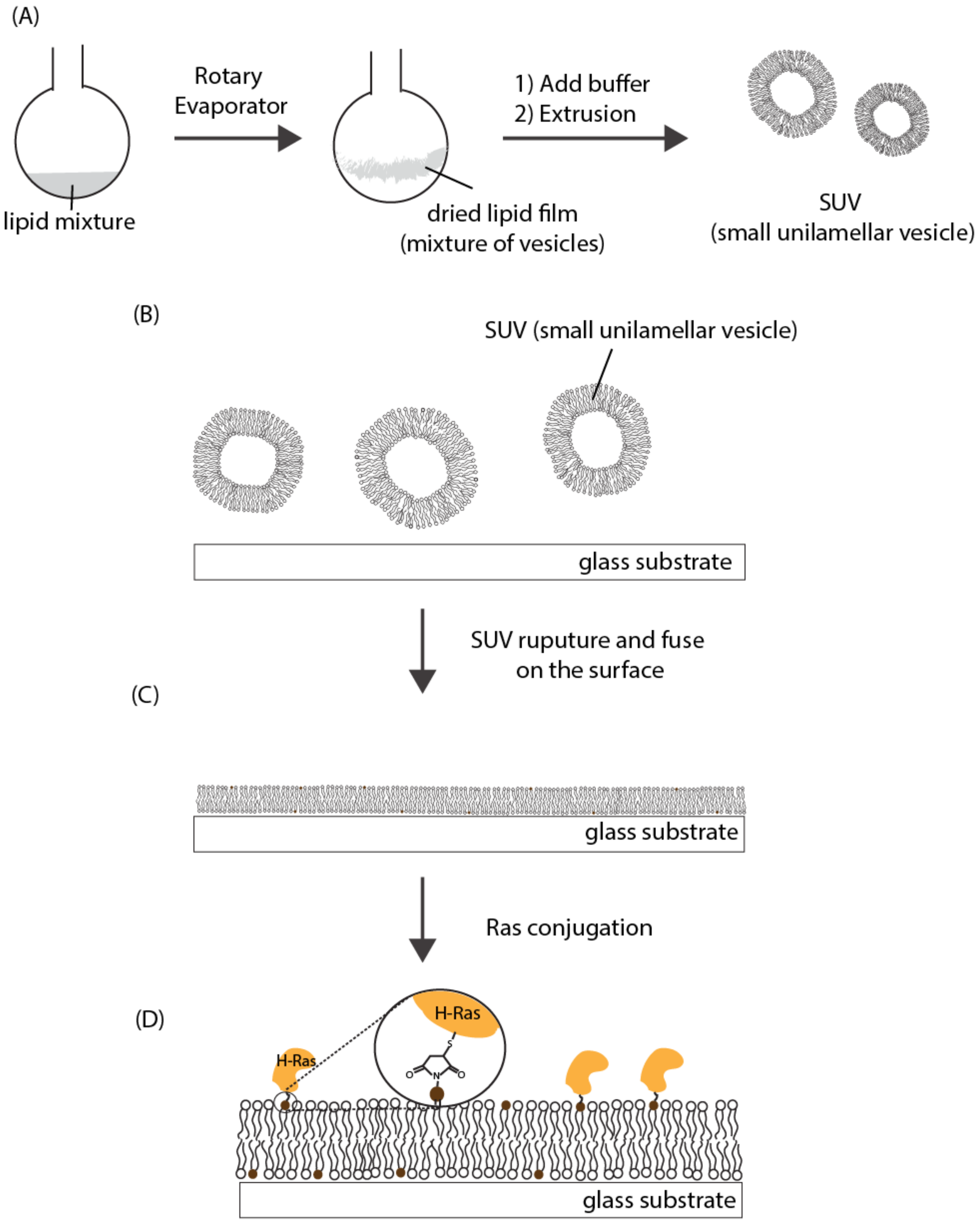

Figure 2-3. A cartoon representation of the formation of supported lipid bilayer. (A) A lipid mixture is mixed at a desired molar ratio. Solvent is quickly evaporated under vacuum and small unilamellar vesicle (SUV) is formed after hydrating and extruding the lipid film. (B) and (C) Supported lipid bilayers is formed by allowing SUVs to spontaneously rupture and self-assemble on the hydrophilic glass surface. (D) H-Ras is functionalized through maleimide and cysteine linkage.

2-6 Study of Ras activation using reconstituted membrane assays

In the following chapters, several supported bilayer assays for studying the activation of small GTPase, specifically H-Ras, were developed and utilized. In chapter 3, I will present the use of fluorescence fluctuation spectroscopy and microscopy to quantitatively characterize membrane-anchored H-Ras on both regular glass slides and micro-patterned substrates. In chapter 4, a detailed kinetic study focusing on the catalytic behavior from hundreds of individual SOS will be described. We found that SOS is very heterogeneous. In addition to observe static heterogeneity which describes the difference between individual enzymes in the same population, we also observed that a single enzyme undergoes state transition with well-defined enzymatic activity at the minute time scale. Moreover, we studied how other biochemical inputs such as lipids and nucleotide state of Ras modulate SOS enzymatic activity and dynamics.

Following the preceding chapters, I will describe the current study on applying various bilayer assays to study the Ras-RasGRP1 interaction in chapter 5. RasGRP1, together with SOS, mediates Ras activation in lymphocytes. The preliminary results suggested that DAG, through the interaction with the C1 domain, increases membrane recruitment of RasGRP1 with high specificity.

Chapter 3 Functionalization and characterization of Ras on the supported membrane

3.1 Introduction

In mammalian signal transduction, Ras functions as a binary switch in fundamental processes including proliferation, differentiation, and survival (*10*). Ras is a membrane-associated protein and serves a network hub; various upstream signaling pathways can activate Ras-GDP to Ras-GTP, which subsequently selects between multiple downstream effectors to elicit a varied but specific biochemical response (*12, 44*). In later chapters of this dissertation, we aim to study the kinetics of Ras activation by its activators, Son of Sevenless (SOS) and Ras guanyl nucleotide-releasing protein (RasGRP), as well as to understand the mechanism of RasGRP membrane localization. Previously, it has shown that the membrane plays a crucial role in governing the kinetics of SOS-catalyzed Ras activation (*26*). As a result, the membrane environment was maintained in all studies of this dissertation.

In this chapter, we used a combination of fluorescence fluctuation spectroscopy and microscopy to quantitatively characterize H-Ras(C118S, 1-181) (referred to as H-Ras from here on) anchored to supported lipid bilayers (SLBs). By tethering H-Ras to membranes at cys181 in the HVR via a membrane-miscible lipid tail, we eliminate effects of lipid anchor clustering while preserving the 15 hypervariable region (HVR) residues between the G-domain and the N-terminal palmitoylation site at cys181 (*26*). Labeling of H-Ras was achieved thought a fluorescent Atto488-linked nucleotide. In addition to functionalize H-Ras to SLBs deposited on regular glass slides, micro-patterned substrates were used to prepare the Ras SLBs (*42*). The chromium diffusion barrier fabricated onto the glass substrate serves as a physical boundary to confine the lateral mobility of surface tethered molecules (lipids and proteins) and allows the design of advanced experiments such as the single molecule kinetic study in the next chapter.

3.2 Results and discussion

3.2.1 Characterization of H-Ras on the supported membrane by FCS, PCH and SMT

In these experiments, H-Ras was attached to the membrane via coupling between cys181 and a maleimide functionalized MCC-DOPE lipid. Since MCC-DOPE is fully miscible in the lipid bilayer, clustering as a result of the lipid anchor itself is avoided.

Two-color fluorescence correlation spectroscopy (FCS) allows the translational mobility of lipids and membrane-linked H-Ras to be monitored simultaneously from the same spot (Fig. 3-1(A) and (B)) (see section 3.3). A small percentage (0.01 mol %) of fluorescent lipid, Texas Red 1,2-dihexadecanoyl-sn-glycero-3-phosphoethanolamine (TR-DHPE), was included in the membrane, while H-Ras is loaded with fluorescent nucleotide, Atto488-GDP or Atto488–GppNp (the nonhydrolyzable GppNp is an analogue of GTP). Normalized autocorrelation functions, $G(\tau)$, of fluorescence fluctuations in the lipid and H-Ras channels are illustrated in Figure 3-1(B). Measured autocorrelation times

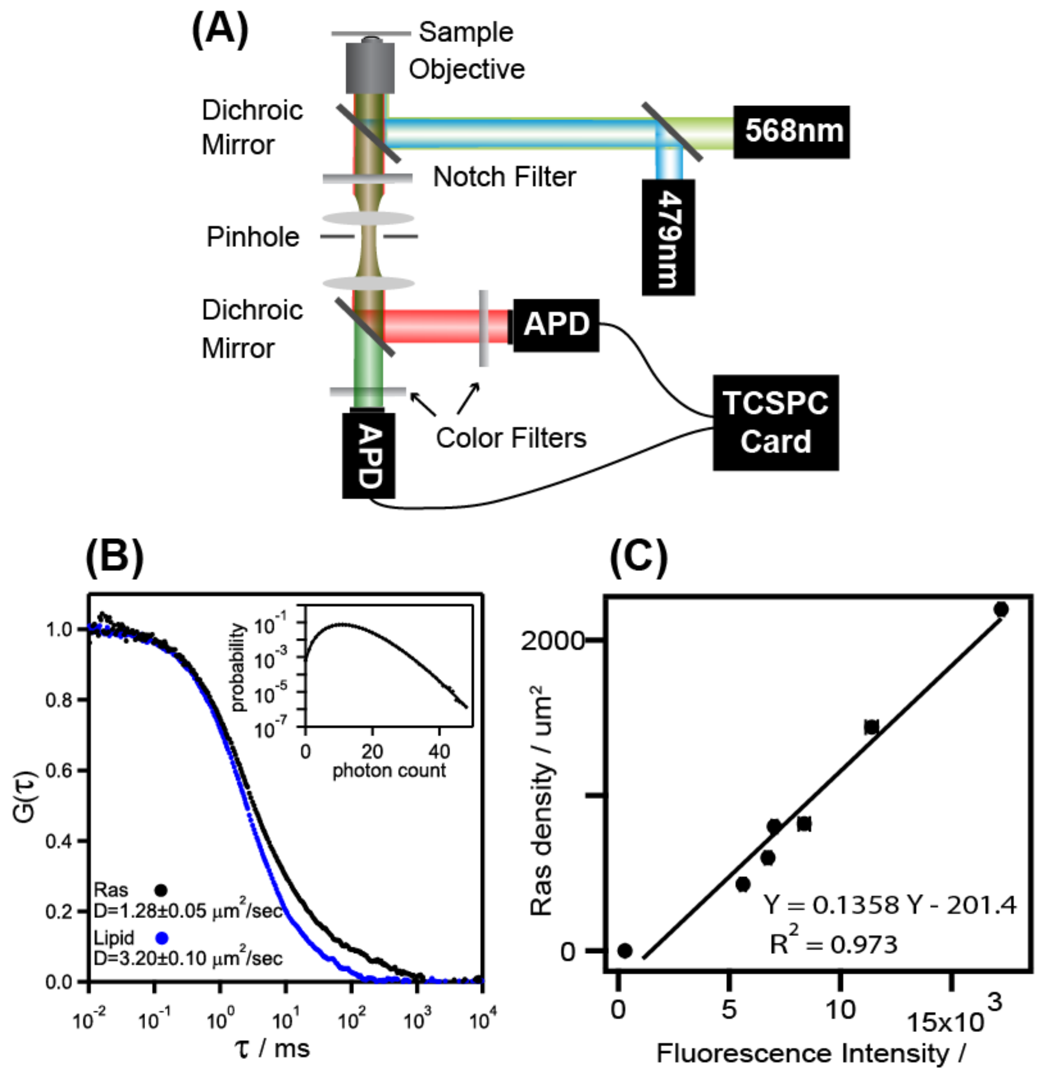

Figure 3-1. Sample characterizations by FCS and PCH. (A) Schematic of two-color FCS setup. (B) Normalized auto-correlation functions, *G*(*t*), of H-Ras and lipid measured simultaneously. Ras displays a slower lateral diffusion compared to lipid. Insert, PCH for Ras on the surface. The analysis gives a surface density of 592 Ras/μm^2. (C) A calibration curve for the conversion between fluorescence intensity and Ras density.

correspond to diffusion coefficients, D, of 3.2 ± 0.1 $\mu m^2/s$ and 1.28 ± 0.05 $\mu m^2/s$ for lipid and H-Ras respectively.

In addition to confirm the two dimensional fluidity of H-Ras samples by FCS, the surface density of Ras can be determined by photon counting histogram (PCH) analysis (see section 3.3). Figure 3-1(C) shows a calibration curve for the conversion between Ras density and observed fluorescence intensity. The calibration curve will be used throughout the dissertation to determine the Ras density.

To probe the distribution of D within the ensemble we used total internal reflection fluorescence (TIRF) microscopy which allows the single molecule tracking (SMT)

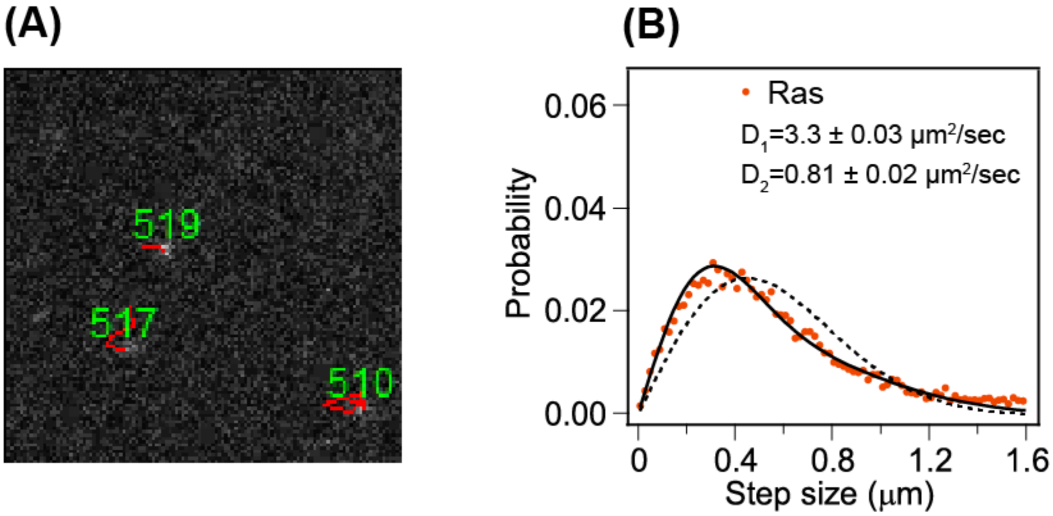

Figure 3-2. Single molecule tracking of H-Ras on the supported membrane. (A) A representative TIRF image of Atto488-GDP loaded H-Ras with particle tracking analysis shown. Red traces represent the diffusion history of individual molecules identified (marked by the numbers) after data analysis. (B) Diffusion step-size histogram from SMT analysis (dots) with diffusion coefficients obtained by fitting data into Einstein diffusion equation. For H-Ras, a two-component model (solid black line) and a single-component model (dashed black line) are shown.

measurements (see section 3.3). With the surface density used here, pre-photobleaching of a field of view is necessary. Fluorescent particles can then be individually resolved and tracked (*45*). Figure 3-2(A) shows a representative TIRF image after tracking analysis (see section 3.3). The diffusion step-size histogram for H-Ras can be determined from a series of TIRF images and is shown in Figure 3-2(B). We inferred D by fitting the step-size distributions to a solution of the Einstein diffusion equation in cylindrical coordinates (please see section 3.3). We found that for H-Ras, a single species model does not fit the diffusion step-size histogram (Fig. 3-2(B), dashed black line), implying that the ensemble contains multiple diffusing species. When a two-species model is used (Fig. 3-2(B), solid black line), the fast diffusing species has a similar D (3.3 ± 0.03 $\mu m^2/s$) to the lipid (Fig. 3-1(B)), while the slow diffusing species has a D of 0.81 ± 0.02 $\mu m^2/s$, which is lower than the average H-Ras D measured by FCS (Fig. 3-1(B)). On membrane surfaces, H-Ras appears to exist as two distinct species. Recently, a study of N-Ras on solid supported bilayers showed that N-Ras forms dimer on the membrane (*46*). We are currently conducting more experiments to see if the distinct H-Ras species observed in our system are dimers/oligomers.

3.2.2 Functionalization of H-Ras on micro-patterned supported lipid membranes

In addition to functionalize H-Ras on the regular glass slide, micro-patterned substrates with chromium diffusion barriers (100 nm in width and 10 nm in height) were utilized (Fig. 3-3(A)) (*42*). Previously, these patterned substrates has been used and found useful in the study of T cell and cancer cell signaling (*47, 48*). Specifically, studies showed

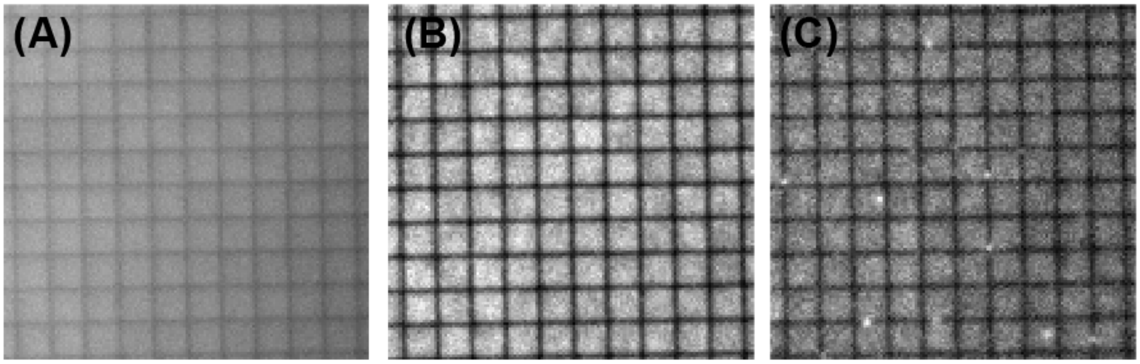

Figure 3-3. H-Ras functionalized supported membrane on a micro-patterned substrate. (A) RICM and epifluorescence images of (B) fluorescent lipid (TR-DHPE) and (C) fluorescent nucleotide-loaded Ras on a patterned substrate. The size of corrals shown here: 2 x 2 μm^2.

that not only the spatial organization of proteins tethered to the lipid membrane was altered but also the downstream signaling was affected (*47, 48*). As I will introduce in the next chapter, a single molecule-enzyme kinetic study of Ras-SOS interaction will be performed. In order to do that, we prepared the SLBs and then functionalized it with H-Ras using the micro-patterned substrate (see section 3.3). Figure 3-3(B) and (C) shows the epifluorescence images of the fluorescent lipid (TR-DHPE) and Atto488-GDP loaded H-Ras respectively, confirming that both lipids and proteins can be partitioned into the individual corrals. In addition, fluorescence recovery after photobleaching (FRAP) measurement was performed at the corner of the patterned area to probe the lateral fluidity of the sample (Fig. 3-4(A) and (B)). The data confirmed that within the patterned area, no recovery was observed after 120s due to the chromium diffusion barrier, whereas clear fluorescence recovery was detected in the area without chromium patterns (Fig. 3-4(C)).

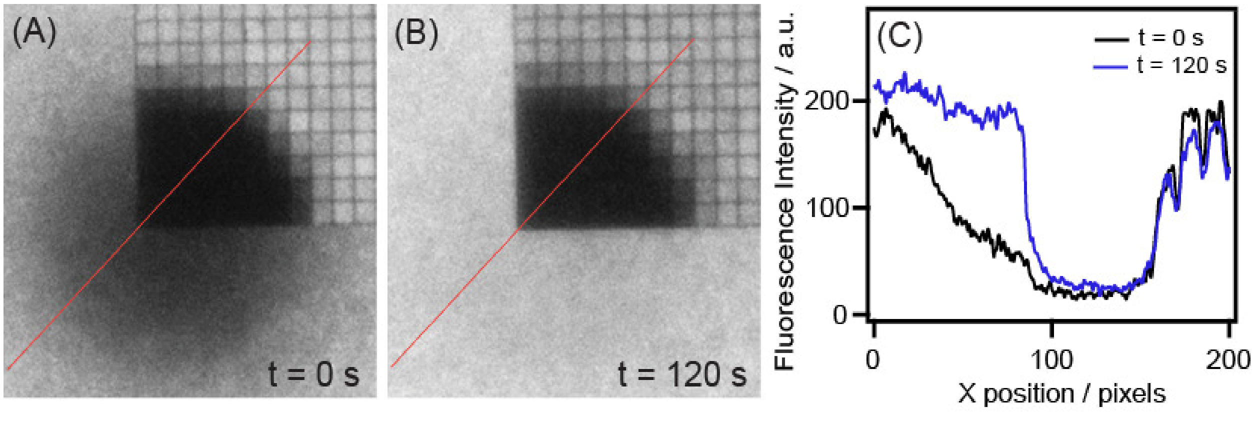

Figure 3-4. FRAP measurement at the corner of the micro-patterned substrate. A Fluorescence recovery after photobleaching (FRAP) experiment performed in order to characterize the mobility of H-Ras. (A) and (B) No fluorescence recovery was observed inside the patterned area due to the chromium diffusion barrier. (C) The fluorescence intensity plot across an identical cross section (red line on (A) and (B)) shows the fluidity of the sample. Size of the corrals: 3 x 3 μm^2.

3.3 Materials and Methods

3.3.1 Chemicals and protein preparation

H-Ras(C181,C118S) (residues 1–181, C118S) was purified as described previously (*26*). The biochemical and structural properties of the H-Ras(C118S) mutant have been characterized with *in vitro* functional assays and NMR spectroscopy, and were found to be indistinguishable from wt H-Ras (*26, 49*). Atto488-labeled guanosine diphosphate (EDA-GDP-Atto488), and Atto488-labeled guanosine triphosphate nonhydrolyzable analog (EDA-GppNp-Atto488) were purchased from Jena Bioscience (Jena, Germany).

3.3.2 Patterned substrates preparation and cleaning

Patterned no. 1.5 thickness glass substrates (Bioptechs) were prepared by e-beam lithography as described previously (*42*). Prior to use, patterned glass substrates were rinsed individually and bath sonicated in IPA/H_2O 1:1, followed by 3 min. piranha etching ($V(H_2SO_4):V(H_2O_2) = 3:1$), and thorough rinsing with copious amounts of ultrapure water. Caution: piranha solution is hot and highly corrosive and can explode if mixed with organic matter. Appropriate safety equipment is required.

3.3.3 Ras functionalized supported lipid membranes

Small unilamellar vesicles (SUVs) were prepared with 93.99 mol % L-α-phosphatidylcholine (Egg-PC), 3 mol % 1,2-dioleoyl-sn-glycero-3-phospho-L-serine (DOPS), 3 mol % 1,2-dioleoyl-sn-glycero-3-phosphoethanolamine-N-[4-(p-maleimido-methyl)cyclohexane-carboxamide] (MCC-DOPE) (Avanti Polar Lipids) and 0.01 mol % TR-DHPE (Life Technologies). All lipids were used from chloroform stocks. Lipids were mixed and chloroform removed by rotary evaporation and N_2 gas drying. The dried lipid film was rehydrated to 1 mg/mL in PBS buffer (pH 7.45). The resulting suspension containing large multilamellar vesicles (LUVs) was then pushed through a polycarbonate membrane with 30nm pore size 11 times using a hand-held extruder (Avestin, Ottawa, ON, Canada).

Immediately after extrusion, the SUVs were deposited on clean glass substrates mounted in flow cells (Bioptechs, Butler, PA) and incubated for 30mins. After the formation of supported lipid bilayers, defects on the bilayers were blocked by a 10 min incubation with 2.5 mg/mL casein in PBS. The bilayers were then functionalized by incubating with 1.3 mg/mL H-Ras in PBS for 2.5 hours at RT, after which the unreacted MCC-PE was quenched by incubating with 5 mM 2-mercaptoethanol for 10 min at RT. The samples were then chilled to 4°C and the buffer exchanged to 40 mM HEPES-NaOH (pH 7.4), 150 mM NaCl. The native nucleotides associated with H-Ras were removed by incubating the samples with a solution containing 50 mM EDTA, 40 mM HEPES-NaOH (pH 7.4) and 150 mM NaCl for 20mins. EDTA buffer was exchanged with (40 mM HEPES-NaOH (pH 7.4), 150 mM NaCl) and fluorescent nucleotides were then loaded onto

H-Ras by an overnight incubation with 10 µM Atto488-GDP or Atto488-GppNp in 40 mM HEPES-NaOH (pH 7.4), 100 mM NaCl, 5 mM MgCl2 at 4°C. Samples were thoroughly rinsed at the end of each incubation with (40 mM HEPES-NaOH (pH 7.4), 100 mM NaCl, 5 mM MgCl2) buffer, and care was taken to ensure that the supported membranes were hydrated at all times.

3.3.4 FCS and PCH

FCS and PCH measurements were acquired simultaneously using a home-built confocal setup on a Nikon Eclipse TE2000-E inverted microscope as described previously (*50*). The TR-DHPE and atto488-nucleotides were excited using a 568nm Kr/Ar ion laser (Newport Corp., Irvine, CA) and a 479nm pulsed diode laser (PicoQuant, Berlin, Germany) respectively, which were combined and coupled into a single-mode optical fiber to ensure overlapping of the two laser lines. The excitation beam was focused by a 100x (1.49 NA) objective lens in the microscope and fluorescence emission was collected through the same objective lens. A custom notch filter (Semrock, Rochester, NY) was used to remove scattered laser light. The emitted light was then passed through a 50 µm confocal pinhole to remove out-of-focus light, split by a 580nm long-pass beamsplitter, and directed toward two avalanche photodiodes (APDs) (Perkin-Elmer, Canada). A short-pass (550 nm) or a band-pass (645/75 nm) color filter (Chroma Technology Corp., Rockingham, VT) was placed in front of each APD to further select the proper wavelengths for green and red channels, respectively. Prior to each experiment, the excitation volume overlap between green and red channels was obtained by carefully aligning the collimator lens placed after the optical fiber and by finely adjusting the objective lens correction collar using a supported lipid bilayer functionalized with GFP-mCherry fusion protein. The excitation volume of the green channel was measured at room temperature (25°C) using a solution of fluorescein (50 nM in 1M NaOH) with known diffusion coefficient (*51*). To obtain the excitation volume of the red channel, the diffusion time constants of the GFP-mCherry fusion protein were first measured in both green and red channels by two-color FCS. The diffusion coefficient of the fusion protein was then calculated from the diffusion time constant in the green channel using the excitation volume of the green channel. Finally, the detection volume of the red channel was obtained from the diffusion coefficient of the fusion protein and the diffusion time constant in the red channel.

Autocorrelation functions (ACFs) were calculated by a hardware correlator (Correlator.com, Bridgewater, NJ) in real time and Igor Pro software (WaveMetrics, Portland, OR) was used for FCS analysis. All ACFs were fitted with a theoretical function describing single species two-dimensional free diffusion. In PCH measurements, the photon arrival times were recorded by a time-correlated single photon-counting (TCSPC) card (PicoQuant, Berlin, Germany) and the histogram of recorded photon counts were later analyzed using the Globals software package developed at the Laboratory for Fluorescence Dynamics at the University of Illinois at Urbana-Champaign.

3.3.5 Single Molecule Imaging and Tracking

Total internal reflection fluorescence (TIRF) experiments were performed on a Nikon Eclipse Ti inverted microscope with a 100× 1.49 NA oil immersion TIRF objective and an iXon EMCCD camera (Andor Technology, UK). 561 nm (Crystalaser, Reno, NV) and 488 nm (Coherent, Santa Clara, CA) diode lasers were used as illumination sources for TIRF imaging. A 60s pre-photobleaching using the strongest power setting of the 488nm laser was performed to create a dark background prior to single molecule imaging. 10 seconds after the pre-photobleaching, a series of TIRF images were then acquired with an exposure time of 10 ms. Single molecule data were quantified employing a custom written particle-tracking analysis suite developed in Igor Pro (Wavemetrics, Oregon, U.S.A.).

Intensity spots originating from individual molecules were localized by thresholding and fitted with a two-dimensional Gaussian function yielding the x and y pixel coordinates for each particle. In this way, lists of particle coordinates were produced for each frame in a time series. Tracks were obtained by linking particles in subsequent frames using a nearest neighbor scheme with a maximum allowed travelled distance of 1.6 μm. A post processing filter was applied to remove immobile particles (defined as average displacement of less than 2 pixels) and unusually dim, or bright, particles. Lists of step-sizes and corresponding time-tags were collected from several time series and samples for each experimental condition and pooled for the diffusion analysis.

3.3.6 Inferring the diffusion coefficient from single molecule tracking data

To calculate the diffusion coefficient, D, from the single molecule Ras tracking data we fitted the data with a simple Brownian diffusion model. The best guess for the model parameter was found using the principle of maximum likelihood. We chose the maximum likelihood approach because (i) it avoids unnecessary binning to produce step-size histograms needed for least squares fitting and (ii) in this modality there is no demand for each observed displacement to have the exact same time interval. The latter was found useful to avoid introducing errors from small variations (millisecond scale) in the timing of image acquisition on our microscope during time-series acquisition and in between samples.

The data consist of observations of particle displacement, r_i, and the corresponding time-interval in which the displacement took place, t_i. We seek to estimate the diffusion constant and the confidence interval associated with this estimate. We assume the data can be described by a simple Brownian diffusion model of the form Eq. S1, with the single model parameter being the diffusion coefficient, D. The measured sets of r_i and t_i can be viewed as discrete samples from the probability density. From a list of r_i and t_i we can infer the optimum value of the model parameter D, corresponding to a particular probability distribution of the form Eq. S1, that would generate the considered data with the highest probability.

The probability density for a particle to move a distance r in time-interval t when the particle can be ascribed diffusion constant D (*52*):

$$\rho(r,t,D) = \frac{r}{2Dt} exp\left(-\frac{r^2}{4Dt}\right) \qquad \text{(S1)}$$

Integrating up in a bin with half width Δ yields the probability to observe a data point with travelled distance r_i and time tag t_i:

$$P(r_i,t_i,D) = \int_{r_i-\Delta}^{r_i+\Delta} \rho(r_i,t_i,D)dr$$

$$P(r_i,t_i,D) = exp\left(-\frac{(r_i-\Delta)^2}{4Dt_i}\right) \text{ - } exp\left(-\frac{(r_i+\Delta)^2}{4Dt_i}\right) \qquad \text{(S2)}$$

From here we can construct the joint probability, i.e., likelihood, of a set of data for different values of our model parameter D:

$$P_J(D) = \prod_i P(r_i,t_i,D) \qquad \text{(S3)}$$

Working with large data sets (hundreds to thousands of steps) the likelihood of observing that particular combination of steps gets infinitely small and computationally impractical to work with. The solution to evaluating P_J (D) in an all at once fashion is to use Bayes rule to recursively update the posterior beliefs on the model parameter D:

$$P(Model|Data) = \frac{P(Model|Data)P(Model)}{P(Data)} \qquad \text{(S4)}$$

Our model is that the data are described by Brownian motion as given by Eq. S1 with an associated value of D. We can now iterate through the data by evaluating Eq. S4 for a chunk of data at a time and continuously update the posterior probability distribution for D, P(Model|Data) = P(D|(r_0; t_0; r_1; t_1…r_i; t_i)). The likelihood of the data given the model, P(Data|Model) = P((r_0; t_0; r_1; t_1…r_i; t_i)|D), is given by Eq. S3. For the first chunk of data we chose a flat prior, P(Model), (expressing maximal ignorance about prior knowledge of the possible value of D) and thus obtain the posterior simply by normalizing the likelihood. We input this posterior as the prior (P(Model)) in evaluating the next chunk of data. In this way we continue iterating through all observed values of r_i and t_i. The denominator in Eq. S4 is simply a normalization factor.

Having taken all data into account, the peak of the posterior, P(D|Data), yields the maximum likelihood estimate on the diffusion coefficient whereas the width of P(D|Data), evaluated as the 95% highest density interval, yields the confidence interval on the inferred D.

We are sampling the posterior numerically on a grid spanning a user defined interval with resolution appropriate to the given set of data. Δ in Eq. S2 is chosen to be orders of magnitude smaller than the resolution of the grid such that there is no practical influence on the result.

H-Ras samples were found to be poorly described by a single component diffusion model but were well fitted with a two-component model. Thus, instead of Eq. S1., we used Eq. S5., where α provides the relative weight of the two populations. In the fitting, α was treated as an independent model parameter.

$$\rho(r,t,D_1,D_2,\alpha) = \frac{\alpha r}{2D_1 t} exp\left(-\frac{r^2}{4D_1 t}\right) + \frac{(1-\alpha)r}{2D_2 t} exp\left(-\frac{r^2}{4D_2 t}\right) \quad \text{(S5)}$$

Chapter 4 Heterogeneity in SOS-catalyzed Ras activation

4.1 Introduction

Cellular membranes organize signal transduction, serving as platforms for protein interactions, as well as direct modulators of enzyme function. Because many signaling pathways converge at the plasma membrane (PM), understanding the coupling between protein function and membrane localization of signaling clusters is of fundamental importance. Modular enzymes at the membrane respond to multiple inputs via simultaneous protein and lipid binding (*3, 53*). At the molecular level, signal integration and subsequent triggering is often achieved by cooperative release of intra-molecular auto-inhibition (*54, 55*), enabling networks to switch, gate and amplify information flow (*56*).

Cytosolic guanine nucleotide exchange factor (GEF) activation of lipid anchored GTPases of the Ras superfamily represents an important class of membrane localized signaling reactions, where regulation proceeds via surface recruitment, in-plane interactions and allosteric control (*57*). GEFs employ a wide array of domain compositions in responding to a broad range of signaling inputs. In spite of this complexity, a recurring feature across several Ras, Rho and Arf GTPase subfamily GEFs is a pattern of regulated release of autoinhibition mediated by GTPase and membrane binding. The molecular mechanisms regulating inhibition and release in these systems remain poorly understood, owing in large part to the difficulty of studying reconstituted membrane systems in vitro. Here, we reconstitute the inner leaflet signaling geometry of Son of Sevenless (SOS) catalyzed nucleotide exchange in H-Ras, using a single enzyme assay to study autoinhibition at the level of SOS specific activity with high throughput.

SOS is widely distributed in mammalian cells. *In vivo*, inactive cytosolic SOS is recruited to the PM in response to receptor tyrosine kinase (RTK) stimulation, where it activates membrane-tethered Ras by catalyzing the exchange of Ras-bound GDP with GTP, triggering the mitogen activated protein kinase (MAPK) cascade (*11*). Ras is a potent oncogene, and SOS activity must be tightly controlled to prevent cellular transformation. SOS is activated by Ras binding to an allosteric site, located between the Cdc25 and REM domains in the catalytic core (SOScat), increasing catalytic activity 75-fold (Fig. 4-1(A)) (*24, 58*). N-terminal Histone fold (H), Dbl-homology (DH) and Pleckstrin homology (PH) domains autoinhibit SOS relative to SOScat. Autoinhibition is thought to occur via steric occlusion of the allosteric site by the DH domain, mediated by intramolecular binding of the H domain to a helical linker connecting the PH and Rem domains (Fig. 4-1(A)) (*25*). A panel of SOS mutations, including R552G in the helical linker, lead to weakened autoinhibition, hyperactive Ras activation and Noonan Syndrome (NS) developmental disorders (*59, 60*). In the present study, SOS constructs derive from truncated SOS-HDPC, which lacks the C-terminal Grb2 binding domain.

SOS responds sensitively to the nucleotide state of Ras (*61*), operating as an analog-to-digital converter via Ras-GTP positive feedback activation (*28, 62*), e.g. during negative selection of maturing thymocytes (*63*). This feed-back loop is thought to involve a combination of recruitment to the PM and allosteric activation once bound there (*26, 64*).

Despite this observation, biological and biochemical studies of SOS activity rely on bulk assays that convolve recruitment and intrinsic activity changes, obscuring the underlying molecular mechanisms of SOS autoinhibition and its pathogenic misregulation. Here, we employ a partitioned supported-membrane presentation of H-Ras (Fig. 4-1(B)) to study how allosteric control of specific activity may regulate Ras-SOS signaling. This presentation allows for precise control and readout of membrane chemical composition and lateral organization. The literal mobility of molecules within the supported membrane is confined in micron-scale corrals by lithographically defined barriers that were prefabricated onto the underlying substrate (*42*). In the present study, barriers restrict surface-tethered Ras and SOS diffusion, while permitting continuous catalytic exchange of

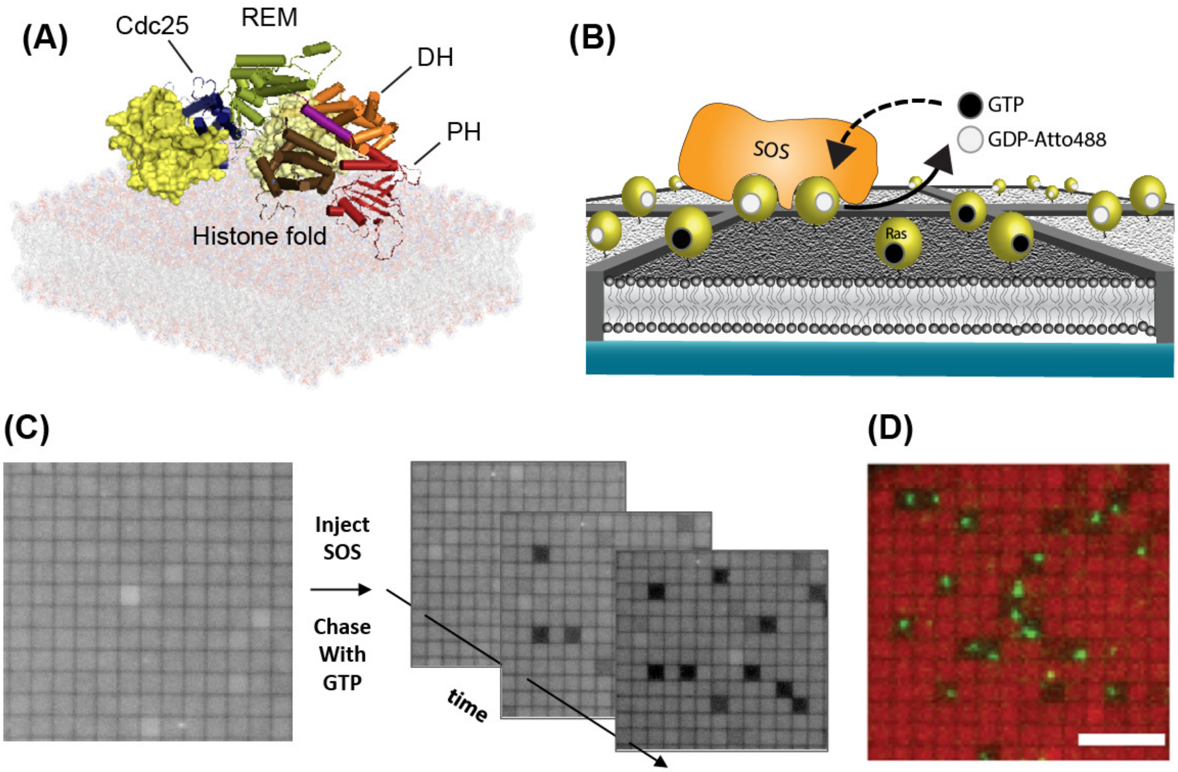

Figure 4-1. Platform for single-enzyme kinetics. (A) Schematic showing the crystal structure and domain architecture of SOS-HDPC (cartoon rendering) with Ras structures (surface rendering) modeled onto the allosteric and catalytic sites, facing a lipid bilayer. SOS-HDPC is depicted in a sterically closed and autoinhibited conformation. The actual on-membrane configuration is expected to be more open. (B) Scheme of the experimental setup. Nanofabricated chromium metal lines (10 nm high, 100 nm wide) partition a supported bilayer into micron-scale corrals, each containing lipid-anchored Ras loaded with fluorescent nucleotide. When a single SOS engages Ras at the allosteric site, the catalytic site is free to turn over the remaining Ras in the corral, replacing fluorescent with non-fluorescent nucleotide, leading to a confined decrease of emission intensity. (C) Widefield epifluorescence image of fluorescently loaded Ras before injection of SOS (*left*) shows no initial dark corrals. Injection of a pulse of SOS followed by continuous flow of non-fluorescent nucleotide (*right*) leads to enzymatic turnover in a sub-set of corrals. (D) False color overlay of fluorescently loaded Ras emission (red) and TIRFM image of fluorescently labeled SOScat-Atto647N (green) reveals co-localization of dark corrals and single SOScat enzymes. The size of corrals in (C) and (D): 2 x 2 μm^2.

fluorescent for non-fluorescent nucleotide supplied via solution in a flow chamber. This geometry has several advantages; (1) SOS can be initially supplied as a transient pulse traveling through the system, ensuring that subsequent turnover is attributable to SOS enzymes that remain surface-bound within the corral array. (2) The SOS concentration in the pulse can be tuned so the majority of catalytically active corrals contain maximally one SOS, ensuring single-enzyme turnover. (3) SOS and Ras within corrals are laterally mobile, allowing SOS to engage lipids, allosteric Ras and catalytic Ras, forming dynamic signaling clusters on the membrane. (4) Ras and SOS surface densities in active corrals remain constant during the reaction, while the percentage of Ras with fluorescent nucleotide decreases due to catalysis, avoiding overall Ras depletion and obviating the requirement for using only initial rates in kinetic analysis.

4.2 Results

4.2.1 Single molecule corral assay

Native H-Ras carries a farnesylated and dipalmitoylated lipid anchor. Here, we employ maleimide coupling of H-Ras(1-181, C118S) (referred to as Ras from hereon) via Cys181 to supported lipid bilayers (SLBs), resulting in stably bound, laterally mobile Ras that is fully functional with respect to SOS activation (*26*). By loading Ras with fluorescent nucleotide (EDA-GDP-Atto488 or EDA-GppNp-Atto488, referred to as GDP-488 and GTP-488 from hereon), catalytic exchange with non-fluorescent nucleotide (GDP or GTP) is directly observed as a local corral-confined decrease of surface fluorescence. Because a constant flow during the exchange reaction ensures removal of unbound fluorescent nucleotides, the reaction kinetics can be recorded with simple wide-field epifluorescence imaging of the fluorescence decay.

Ras surface densities were adjusted between several hundred and a thousand Ras μm^{-2}, corresponding to the broad Ras density range measured *in vivo*. Ras surface density was calibrated with fluorescence correlation spectroscopy (FCS) and subsequently measured by imaging with epifluorescence microscopy (Fig. 3-1(C) in chapter 3). Measurement of Ras lateral mobility with FCS and fluorescence recovery after photobleaching (FRAP) (Fig. 3-4 in chapter 3) ensured that fluid bilayers were partitioned by leak-free corrals.

Representative images taken during SOScat-catalyzed turnover show a small percentage of 'active' corrals undergoing nucleotide exchange, developing a clear negative contrast relative to 'inactive' bright corrals (Fig. 4-1(C)). Total internal reflection fluorescence microscopy (TIRFM) of Atto647N labeled SOScat (SOScat-647) reveals a clear correspondence between active dark corrals and individually confined SOScat enzymes (Fig. 4-1(D)). In all experiments, SOS concentrations were adjusted so that >95% of active corrals contained 1 enzyme. Because injected SOS binds the membrane surface at random lateral positions, at a given average surface density the corral occupancy of SOS follows a Poissonian distribution. Therefore, a statistically equivalent requirement to

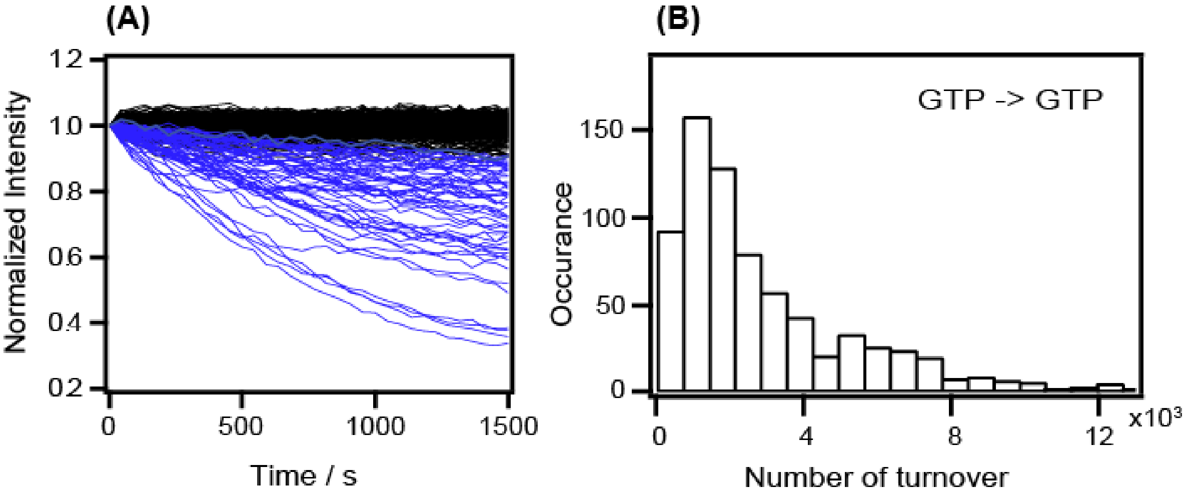

Figure 4-2. **Normalized raw intensity traces and total turnovers catalyzed by one SOScat.** (A) Collection of normalized single-corral kinetic traces from an array of SOScat turning over Ras-GTP, showing the percentage of fluorescent Ras in the corral as a function of time (blue traces). The black traces represent signals from corrals without enzymatic activity. (B) Single SOScat enzymes catalyze hundreds to thousands of nucleotide exchanges. Histogram of number of exchanges measured from the single molecule corral assay.

having only a single SOS in an active corral with ~95% probability is that ~10% or less of all corrals in the array are enzymatically active (turn dark) during turnover. Importantly, this internal control allowed us to reliably monitor single-enzyme kinetics (in >95% of traces) even for non-fluorescent SOS constructs. By imaging arrays of corrals on the surface, the exchange reactions of hundreds of individually confined enzymes can be monitored in parallel. Quantitative analysis of fluorescence decays (see section 4.5 for further discussion) allows individual kinetic traces of SOS activity to be analyzed (Fig. 4-2(A)), providing information on single-enzyme properties across the ensemble. SOScat is known to exhibit accelerated catalysis in bulk assays when Ras is presented on vesicle membranes instead of in homogeneous solution. Single enzyme kinetic traces of continuous SOScat catalysis presented here is direct evidence that SOScat enzymes can be highly processive, each turning over hundreds to several thousand Ras while residing on the membrane (Fig. 4-2(B)). A W729E point mutation in SOScat (SOScat(W729E)), previously found to abolish Ras binding in the allosteric pocket, inhibits detectable pattern formation in the array, confirming that the processive phenotype requires an intact allosteric site (data not shown).

4.2.2 Dynamic heterogeneity and allosteric regulation by N-terminal domains

Changes in the internal dynamics of enzymes is a potent allosteric modulator of biochemical activity (*65*), via induced changes in the protein conformational entropy (*66*) and the sampling of 'long-lived' poorly populated protein states (*67*). Slow conformational fluctuations are traditionally observed on the microsecond to millisecond time-scale (*65, 68, 69*), but it is becoming clear that longer-lived dynamic conformers exist in proteins

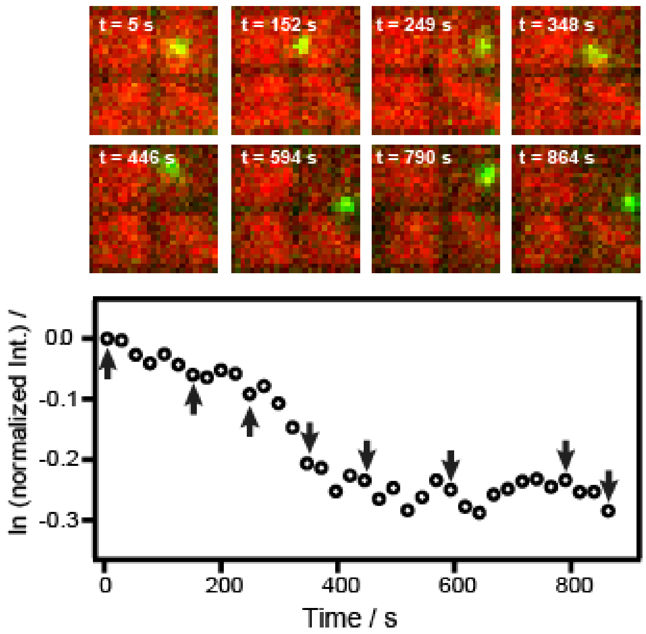

Figure 4-3. Dynamic heterogeneity is not due to hindered SOScat diffusion. In this experiment, we measured the nucleotide exchange reaction by one epifluorescence image (red channel), followed by 3 consecutive TIRF images which allow the monitoring of SOScat diffusion (green channel) every 35-40 seconds. (Top) The overlaid images of fluorescence and TIRF image at various time points. We did not observe the enzyme being trapped or became immobile in this experiment. (Bottom) The kinetic trace extracted from the corresponding corral (upper right) shows the enzyme exhibited different catalytic rates during the course of exchange reaction. Arrow indicates the corresponding time point shown on the top.

(*70*). For signaling proteins, dynamic properties are likely to play a major regulatory role (*71*). For example, in the Rac GEF Vav1, release of autoinhibition by phosphorylation happens via stochastic fluctuations to a sparsely populated state (*72*). Molecular dynamics (MD) simulations of SOScat predict similar fluctuations in the allosteric and catalytic sites, between inactive and active states, and show that protein flexibility in SOScat may be important for allosteric regulation of SOS (*73*). In order to study SOS dynamics, we analyzed individual kinetic traces for the existence of activity fluctuations, using a change-point detection algorithm (see section 4.5.3 for discussion). This analysis reveals that SOScat enzymes can fluctuate between distinct long-lived (>100s) functional states, identified as linear segments in logarithmic plots of Ras turnover (Fig. 4-5(A)). These long-lived states may contain additional tiers of rapidly interconverting substrates, which are not resolved experimentally. Some SOScat enzymes remain in a single state for the duration of the experiment (>20 min) while others transition between different activity states, sometimes repeatedly. Changes in turnover rate are not associated with changes in lateral diffusion (Fig. 4-3). The log-plot slopes each define a fluorescence decay rate constant k_{app}, which gives the corresponding state turnover number TN via $TN=k_{app}*[Ras]_0$, where $[Ras]_0$ is the total amount of Ras in the corral (see section 4.5.2 for discussion). In the following, 'TN' and 'rate' are used interchangeably. For all sample configurations tested, the Ras density dependence of SOS TN is dominated by a large degree of state to state variation (Fig. 4-4). This shows that individual activity levels and transitions between them are intrinsic characteristics of membrane-bound Ras-SOS complexes. We therefore interpret TN variation as arising from fluctuations in either k_{cat}, K_M or both. In the following, rate histograms with broadly overlapping Ras densities below 1000 Ras/μm^2 are used for comparisons between constructs, unless explicitly noted.

Dynamic heterogeneity has been reported for multiple enzymes (*74*). However, the duration of dynamic SOS states (several minutes, see Fig 4-7(B)) is significantly longer than previous reports of enzyme states, lasting up to tens of seconds (*75, 76*). Historically, ultra long-lived excited protein states have been invoked to explain bulk enzyme hysteresis (*77*) on the minute to hour time-scale (*78, 79*). The SOScat fluctuation behavior shows that dynamic conformational modes in signaling enzymes may extend well into timescales relevant for complex cellular processes, or even the lifetime of the protein itself (*80*). This is significant, since stochastic transitions between long-lived states may encode specific information processing capabilities in the signaling network (*81*).

By identifying individual functional sub-states, we can construct the life-time weighted probability histogram of TNs sampled by hundreds of SOScat enzymes (Fig. 4-5(B) and see section 4.5 for further discussion). The histogram spans almost 2 orders of magnitude, with a broad peak at ~1s^{-1} and a wide shoulder and tail of sparsely populated

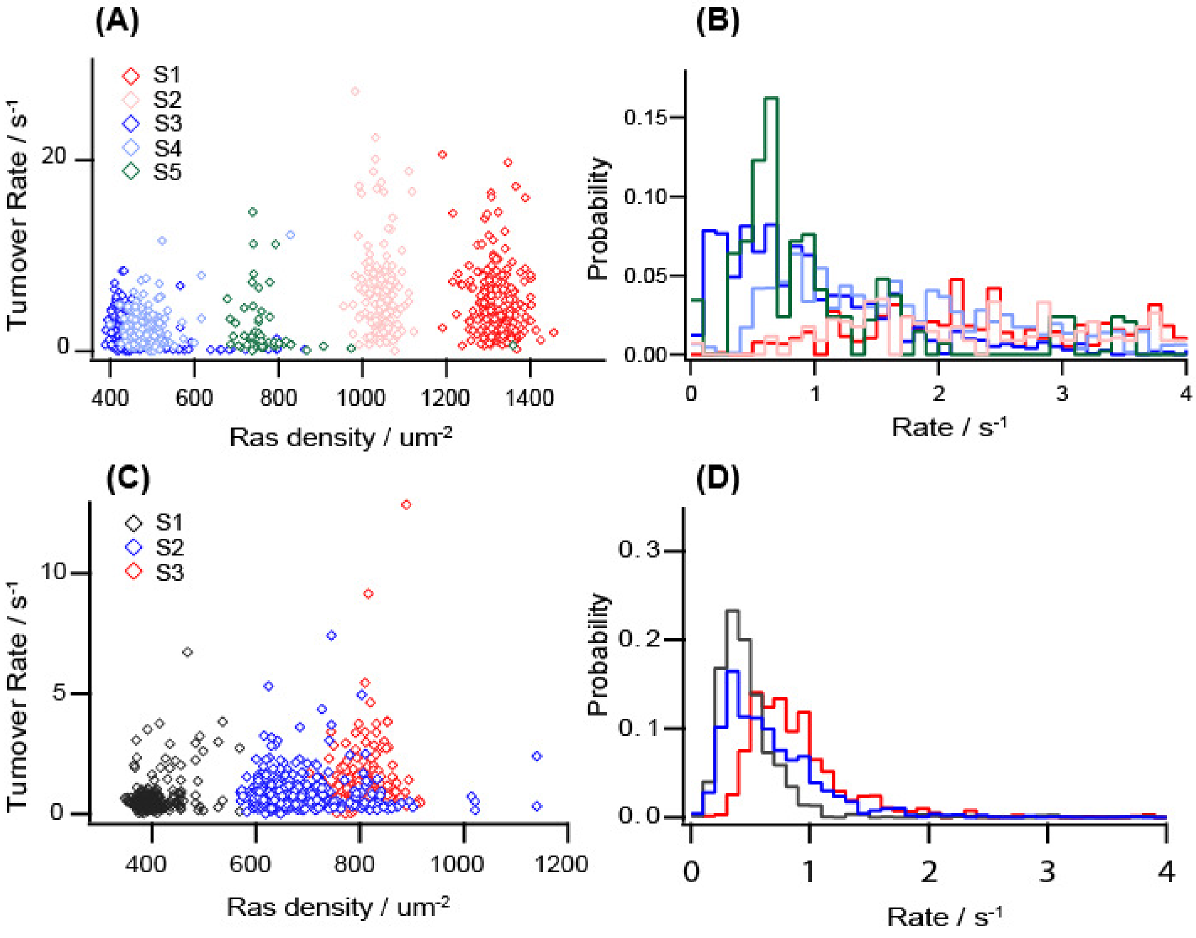

Figure 4-4. SOScat and SOS-HDPC exchange rate dependency on Ras density is dominated by intrinsic variation. Shown here is data collected from Ras-GTP to GTP exchange reaction. (A) and (C) show the Ras density-dependency of SOScat and SOS-HDPC catalyzed turnover rates. (B) and (D) show the corresponding exchange rate histograms for individual samples. The data suggesting that there is a tendency of histogram broadening with increasing Ras density. Notice that only rate below 4 turnovers/s is shown in (B).

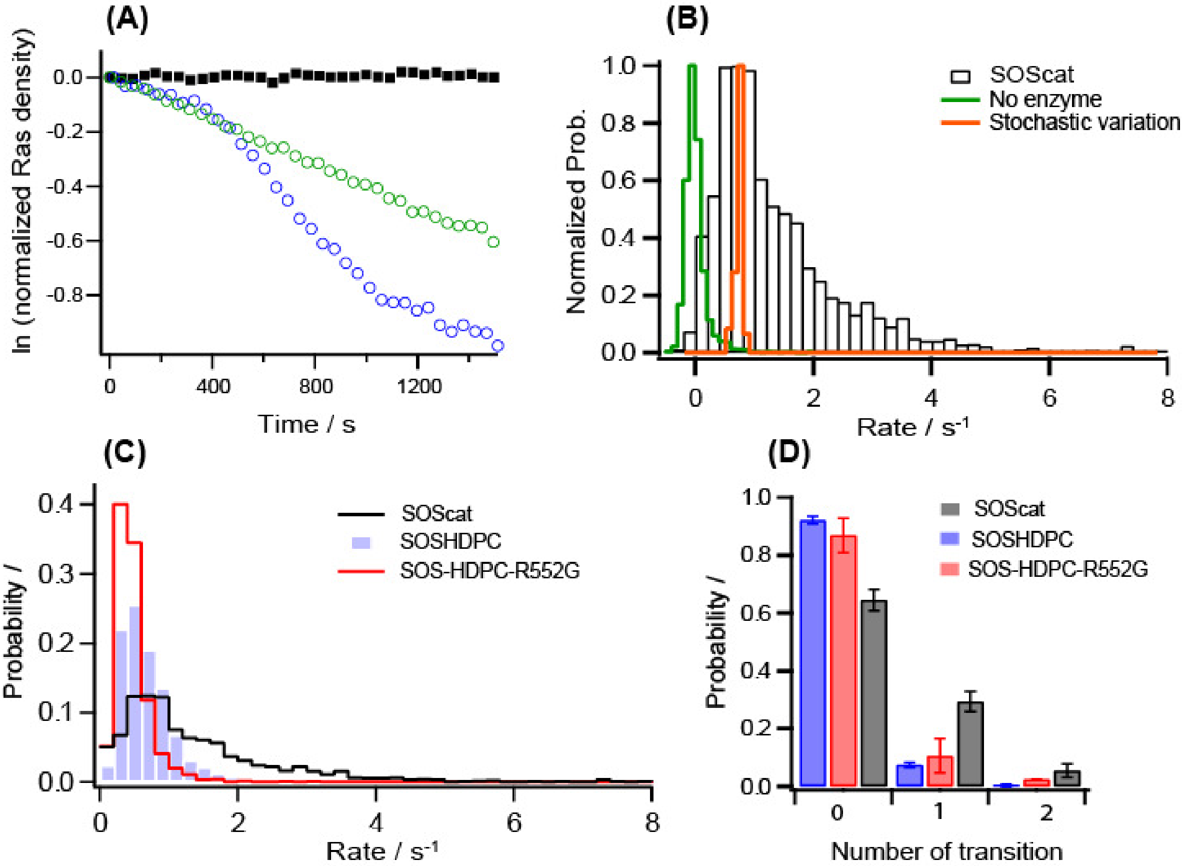

Figure 4-5. Allosteric autoinhibition by N-terminal domains. (**A**) Logarithmic plots of single enzyme kinetic traces. Discrete activity levels of SOScat are identified as linear segments. Some SOScat enzymes remain in a single functional state throughout the reaction (green *straight trace*), while others fluctuate between different states (*blue kinked trace*). (**B**) Normalized and lifetime-weighted turnover number probability distribution of states sampled by (i) the SOScat ensemble (black), (ii) corrals without enzyme (green) and (iii) modeled single-state enzyme stochastic variation (red). (**C**) Turnover number probability distributions from SOScat (black), SOS-HDPC (blue) and SOS-HDPC(R552G) (red). The N-terminal domains autoinhibit SOS specific activity. A Noonan syndrome associated point mutation in SOS-HDPC(R552G) (red) does not relieve inhibition. (**D**) State transition frequency probabilities for SOScat (black), SOS-HDPC (blue) and SOS-HDPC(R552G) (red). N-terminal domains reduce the fluctuation frequency relative to SOScat (Ras densities below 1000 molecules/μm^2 were used).

states extending toward higher rates. The rate histogram of inactive corrals (without enzyme) is plotted in the same graph, centered at zero. Histograms are normalized, in order to compare distribution widths. The inactive corral histogram arises from intrinsic nucleotide release and photobleaching and represents the narrowest distribution resolvable with the experimental setup (See section 4.6 for further discussion). The SOScat distribution is an order of magnitude broader, suggesting that SOScat enzymes sample multiple distinct catalytic states. Likely, the assay does not resolve individual state peaks, giving instead the appearance of a broad continuous distribution. The catalytic cycle of SOS is characterized by a branched network of molecular transitions, related to binding, unbinding and turnover at the two Ras binding sites (*26*) (Fig. 4-12). Even in a simplest-case single-state SOScat system, random path selection in this reaction network will lead

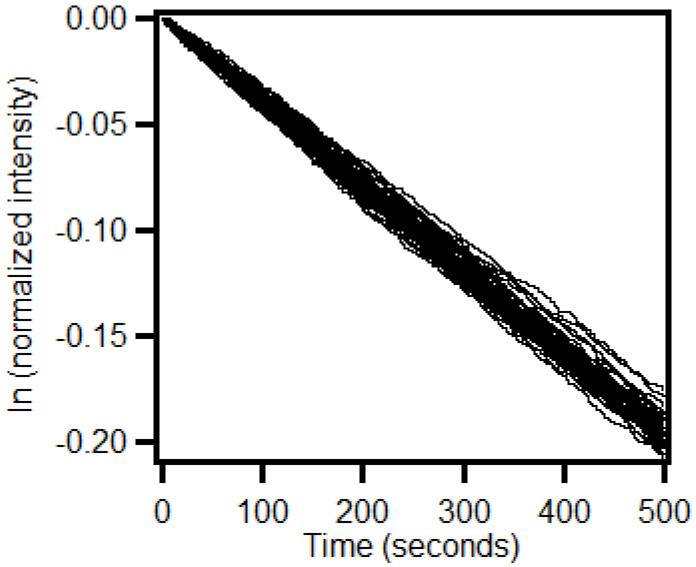

Figure 4-6. **Representative simulated kinetic traces.** 50 representative kinetic traces obtained from stochastic simulation based on the model shown in Figure 4-12. Please see section 3.6 for parameters used in the simulation.

to stochastic variation in turnover rate over time and between enzymes. In order to estimate the distribution width associated with this variation, we used literature estimates of SOScat rate parameters to perform stochastic simulations (See section 4.6 for discussion and Fig. 4-6). The rate distribution resulting from 500 simulation runs is plotted on Figure 4-5(B), showing that stochastic variation in a 'one-state' system does not account for the experimental distribution width. Together, these histograms show that processive SOScat enzymes can access a range of functional states, resulting in a wide rate distribution that allows more than 10-fold allosteric activation. Analysis of states from single traces shows that individual enzymes can sample states across the full ensemble distribution. We conclude that stochastic conformational fluctuations in SOScat generate distinct long-lived functional states.

A key finding comes from a comparison of rate histograms for SOScat and SOS-HDPC (Fig. 4-5(C)). The N-terminal H-DH-PH domains have a pronounced effect on the distribution of rates sampled by SOS; while the peak is minimally shifted toward lower rates, the shoulder and extended tail are strongly suppressed, resulting in a sharper histogram. As shown in Figure 4-5(D), the N-terminal domains also dampen the frequency with which sampling occurs. For SOScat turning over Ras-GDP, 35% of all enzymes undergo state transitions, dropping to 10% for SOS-HDPC. We conclude that the N-terminal domains autoinhibit SOS activity in the functional Ras-bound state on the membrane, by allosterically suppressing fluctuations that populate multiple high activity states, consistent with a mechanism of conformational selection. This represents a previously unknown layer of SOS regulation and emphasizes that not just the allosteric site, but also the N-terminal domains, communicate directly with the catalytic site.

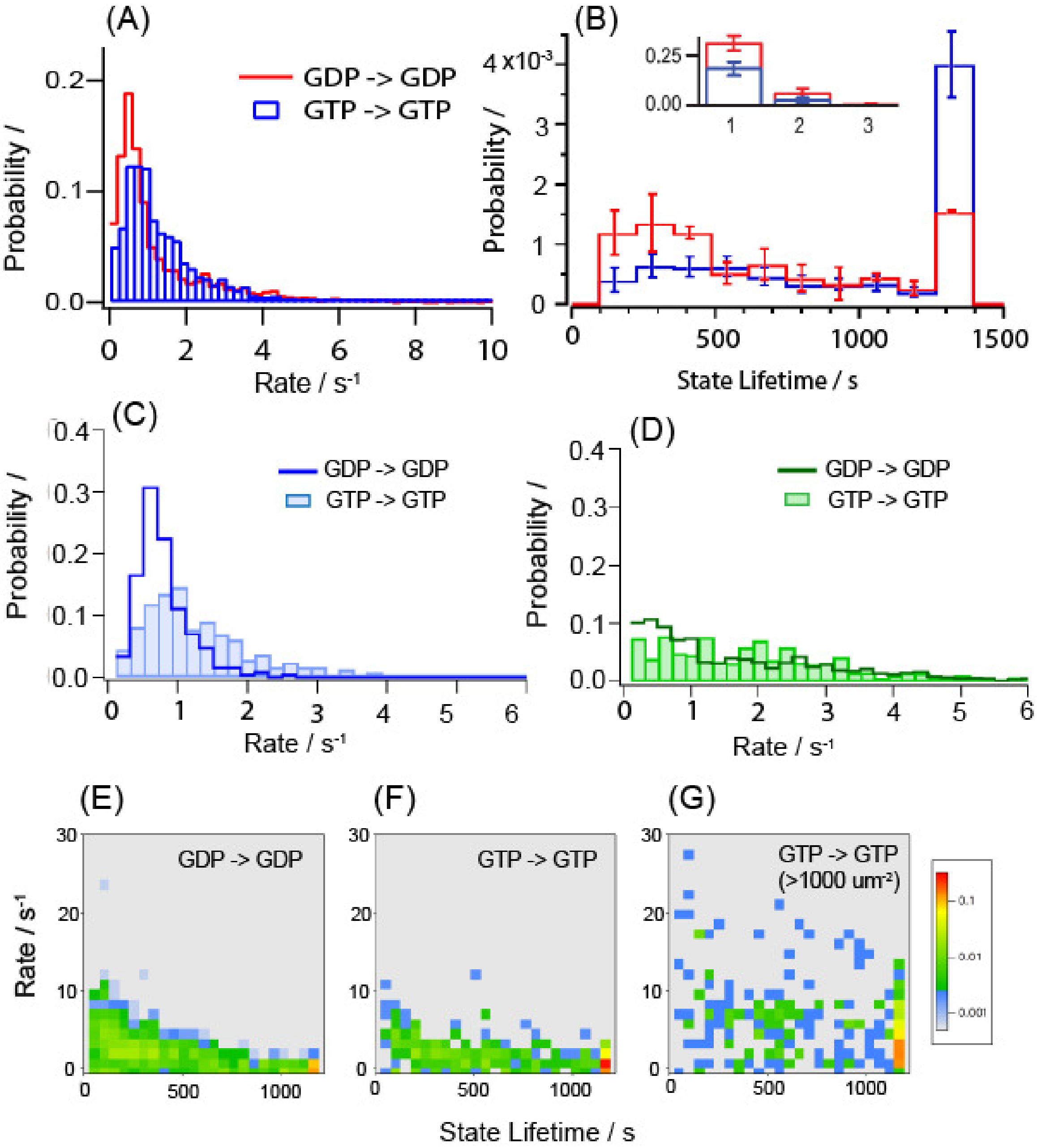

Figure 4-7. Nucleotide specificity of SOScat. (**A**) SOScat TN probability distributions for Ras-GDP-Atto488 (red) and Ras-GTP-Atto488 (blue). (Ras densities below 1000 molecules/μm^2 were used). (**B**) SOScat state lifetime probability distributions for Ras-GDP-Atto488 (red) and Ras-GTP-Atto488 (blue). The final bin represents states longer than the duration of a full experiment. Inset: SOScat state transition frequency probabilities for Ras-GDP-Atto488 (red) and Ras-GTP-Atto488 (blue). (**C**) TN probability distributions for static SOScat (enzymes without fluctuations) on Ras-GDP-Atto488 (line) and Ras-GTP-Atto488 (bar). (**C**) TN probability distributions for dynamic SOScat (enzyme with fluctuations) on Ras-GDP-Atto488 (line) and Ras-GTP-Atto488 (bar). (**E**), (**F**) and (**G**) Probability distribution maps of SOScat state lifetime and TN for Ras-GDP-Atto488 (E), Ras-GTP-Atto488 (F) and Ras-GTP-Atto488 above 1000 Ras/μm^2 (G). Color bar is log-scale.

The Noonan syndrome associated R552G mutation in the helical linker of SOS leads to sustained and excessive Ras activation *in vivo* (*59, 60*) and is known to increase the apparent rate of catalysis in bulk assays, but only in a membrane context (*26*). To investigate the effect of the R552G point mutation on SOS, we tested SOS-HDPC(R552G) in the corral assay. Interestingly, the resulting rate histogram shows that the R552G mutation is not activating at the level of SOS specific activity (Fig. 4-5(C)) and results in a similar low fluctuation frequency as seen for SOS-HDPC. This demonstrates that accelerated turnover of Ras-GTP by SOS-HDPC(R552G), previously reported for bulk vesicle assays, is a result of increased surface binding from solution, and suggests that pathogenic hyper-activation of Ras signaling *in vivo* is at least partially a result of abnormally high membrane recruitment of SOS(R552G).

4.3.3 Dependency of turnover rate on nucleotide state of Ras and lipids

An important aspect of SOS biology is the nucleotide specific regulation of signaling activity. SOS signaling is amplified by conversion of Ras-GDP to Ras-GTP *in vivo* (*61*) and increased apparent rates of turnover for Ras-GTP have been observed *in vitro* (*24*). These findings have motivated the hypothesis that SOS activation and Ras-GTP formation create a positive feedback loop at the membrane (*28*), but the molecular mechanisms underlying this network switch remain unclear, and both surface recruitment and allosteric activation have been implicated. In order to study the nucleotide specificity of SOS, we loaded Ras with either GTP-488 or GDP-488, followed by catalytic replacement with identical but non-fluorescent nucleotide, ensuring that Ras maintained the same nucleotide state throughout the experiment.

An interesting finding comes from the nucleotide comparison of SOScat. SOS nucleotide specificity is known to propagate from the allosteric site of the catalytic core, but the mechanism has been controversial (*24, 25*). As shown in Figure 4-7, we find that the effect of nucleotide state on SOScat activity is subtle. Overall, the GDP and GTP rate histograms largely overlap, but reveal a redistribution of states from the GDP peak at 1 turnover/s^{-1} to the GTP shoulder at 2 turnover/s^{-1} (Fig. 4-7(A)). This shift is accompanied by a nucleotide-induced change of the SOScat state lifetime distribution (Fig. 4-7(B)). As shown in the in-set, Ras-GTP in the allosteric site stabilizes the Ras-SOScat complex and reduces the fluctuation frequency between states. This leads to a depletion of ‘dynamic’ shorter-lived states below 500s and a corresponding increase in ‘static’ longer-lived states that remain unchanged for the duration of the experiment (1220s or more).

The conformational dynamics of Ras regulate signaling specificity (*82*) and are strongly affected by the bound nucleotide and Ras-membrane interactions (*83*); Ras-GDP shows increased structural flexibility relative to Ras-GTP, especially in the effector interaction regions switch I and switch II, where also SOS binds Ras (*84*). For example, GTP loaded Ras fluctuates between two distinct switch II region conformations on the ms timescale (*85*). Our results show that the allosteric site of SOScat acts as a sensor of

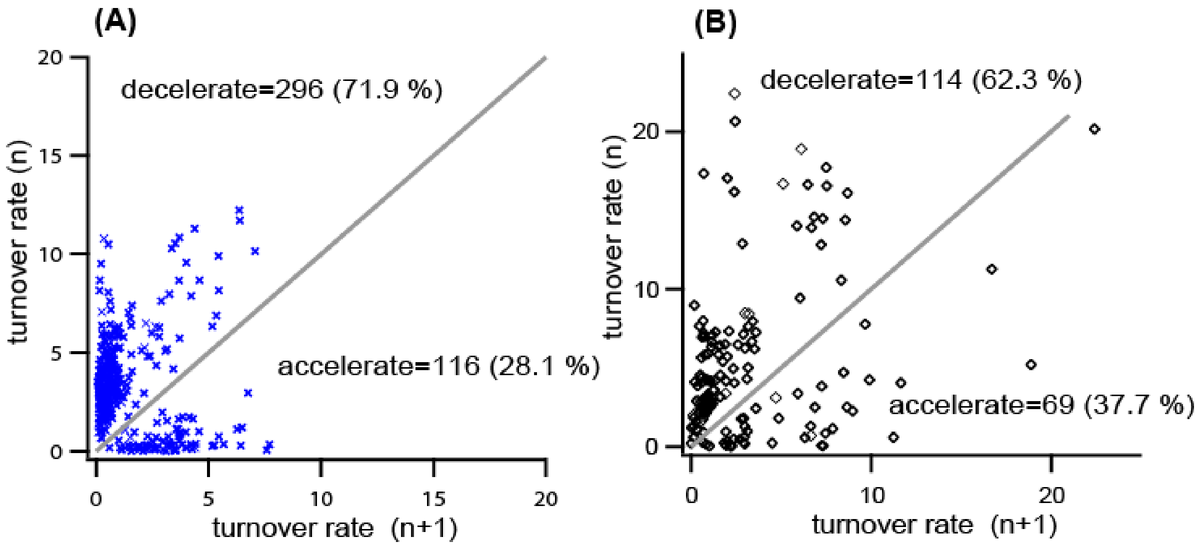

Figure 4-8. Fluctuation path plots for SOScat. For each state transition, the initial rate (n) is plotted against the subsequent state rate (n+1). Points above the diagonal correspond to rate decrease and vice versa. (A) Ras-GDP promotes SOScat fluctuations into lower activity states 72% of the time, primarily into a basal state with a rate close to 1 turnover/s^{-1}. (B) Ras-GTP shows a similar pattern, albeit with a 10% shift toward fluctuations into higher activity states.

conformational dynamics, translating intrinsic millisecond fluctuations of Ras into 5 orders of magnitude slower functional fluctuations of the membrane-bound Ras-SOS complex.

To further explore heterogeneities between ensemble subsets, the nucleotide specific rate histograms of static and dynamic states of SOScat are plotted (Fig. 4-7(C) and (D)). This reveals that nucleotide specific redistribution of specific activity is almost fully mediated by static SOScat enzymes (Fig. 4-7(C)), whereas fluctuating enzymes sample distributions that are close to nucleotide-independent (Fig. 4-7(D)). In addition, the rate distributions of static and dynamic SOScat enzymes are different; the static subset populates relatively narrow distributions that peak around 1 turnover/s^{-1}, whereas the dynamic subset displays flat and broadened distributions with tails extending to higher rates. These results suggest that, upon binding to Ras on the membrane, processive SOScat forms a highly non-ergodic ensemble, populating a nucleotide-dependent conformational landscape sampled by rare fluctuations between kinetically trapped, long-lived states. If solution-phase SOScat engages Ras in the allosteric site via conformations away from equilibrium of the resulting Ras-SOS complex, subsequent fluctuations are expected, on average, to funnel the complexes toward a native state. Such behavior is observed in the anisotropic fluctuation path plot of SOScat (Fig. 4-8), which shows that the majority of state transitions lead to a reduction in catalytic rate, with the strongest fluctuation channel leading to the lowest-activity state. This suggests that, upon membrane binding, the overall SOScat ensemble is gradually slowing down as a low-activity native state is approached.

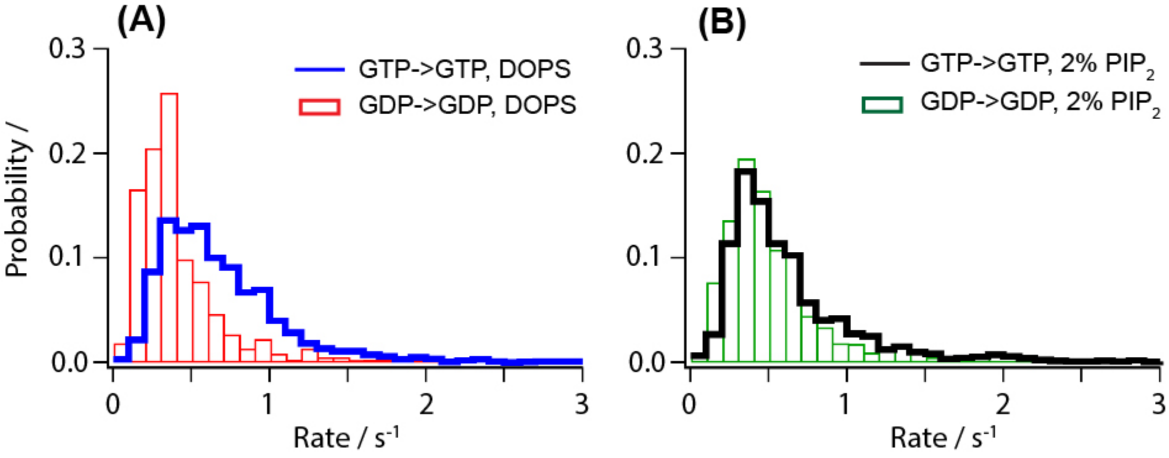

Figure 4-9. Influence of PIP_2 lipids on SOS-HDPC. (A) and (B) SOS-HDPC turnover number probability distributions for bilayers without (A) or with (B) 2% PIP_2 lipids. On bilayers without PIP_2 (A), SOS-HDPC has a broader distribution when turning over Ras-GTP-Atto488 (blue) compared Ras-GTP-Atto488 (red). In contrast, on 2% PIP_2 containing bilayers (B) the two nucleotide configurations have overlapping distributions (green and black).

The interplay of rate and lifetime is shown in two-dimensional probability maps for Ras-GDP and Ras-GTP in Figure 4-7(E) and (F). These ‘activity-landscapes’ serve as fingerprints of SOScat functional dynamics. In both nucleotide configurations, highly active states correlate with short lifetimes (app. 200s). The maps show that Ras-GTP allosterically promotes long-lived states at the expense of low-activity shorter-lived states. Surprisingly, we find that high Ras surface densities (above 1000 Ras/µm2) lead to a pronounced redistribution of SOScat activity toward higher rates, especially for longer-lived states. A gradual transition from non-saturating (kcat/Km limited rate) to saturating

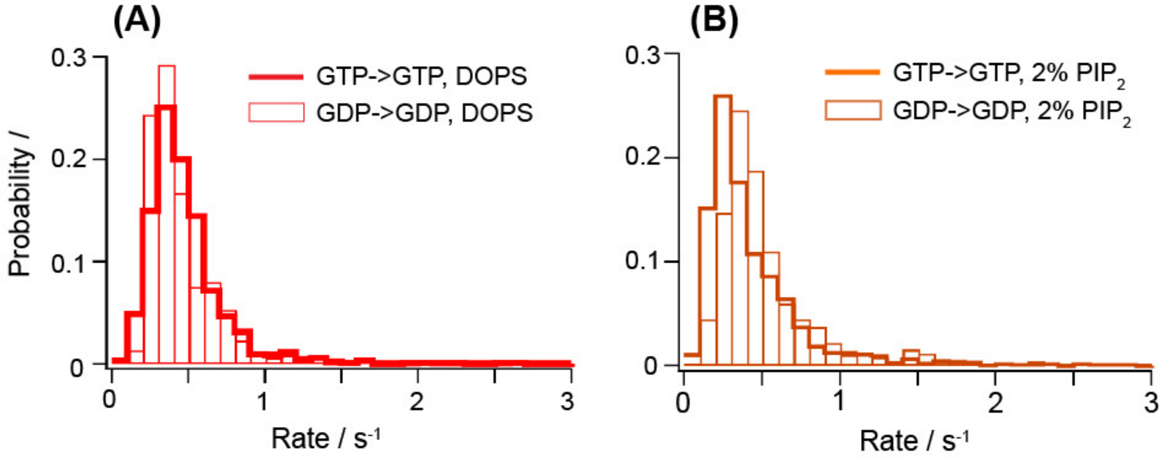

Figure 4-10. **Sensitivity of SOS-HDPC(R552G) towards nucleotide state of Ras and PIP_2 lipid.** Noonan syndrome related SOS-HDPC(R552G) is irresponsive to both (A) Ras nucleotide state and (B) PIP_2 lipids, with respect to specific activity.

(kcat limited rate) Ras densities for the high activity states could contribute to this broadening.

Similar nucleotide dependence is observed for SOS-HDPC, albeit shifted to lower rates by the autoinhibitory domains (Fig. 4-9(A)). Interestingly, the SOS-HDPC(R552G) construct does not display sensitivity to the nucleotide state of Ras (Fig. 4-10(A)). At the level of SOS specific activity, lack of nucleotide regulation rather than increased activity may contribute to aberrant signaling by the R552G mutant. SOS has been shown to bind PIP_2 lipids via the PH domain (*26*), relieving autoinhibition and increasing overall rates in bulk vesicle assays, but the effect on specific activity is unknown. As shown in Figure 4-9(A) and (B), the presence of 2% PIP_2 in the bilayer does not appreciably increase SOS-HDPC specific activity. Instead, PIP_2 appears to remove the nucleotide difference observed for SOS-HDPC on bilayers without PIP_2 (Fig. 4-9(B)). This shows that the reported activating effect of PIP_2 on SOS signaling happens by increased surface recruitment rather than via allosteric activation of specific activity.

4.3 Discussion

What is the biological significance of rare, long-lived, high activity states in SOS? Evolutionary pressure is required to evolve and maintain increased enzymatic efficiency (*86*), so high activity states are likely to be biologically important. For some autoinhibited enzymes with rare excited states, mutations (*67*) or allosteric interactions (*72*) are known, which reshape the energy landscape such that the rare state becomes predominant. We cannot exclude that such inputs exist for SOS, e.g. phosphorylation, binding to activated RTKs via the Grb2 domain or other interactions, which would strongly activate GEF activity by preferentially populating high-activity states.

However, rare states could be a specifically evolved characteristic of SOS, as indicated by our findings that allosteric regulation by the N-terminal domains and allosteric Ras serves to gradually reshape the rate distribution tail, rather than switching the entire ensemble between states. In vivo, a wide distribution of active states would effectively serve to introduce noise in the biochemical signal of Ras activation. Endogenous sources of cellular stochasticity can drive biological processes (*87*). For example, the functional role of noise in regulating genetic circuits is well established (*88*). Fluctuations in copy number of certain proteins are a key source of noise used in decision-making and adaptive processes (*89*), and dynamic activity fluctuations within a heterogeneous enzyme ensemble could serve a similar purpose (*90*). An important biological function of stochastic fluctuations in enzyme activity is to trigger phenotype switching in bimodal cells (*91*). Even a single rare stochastic event like repressor dissociation from its operator DNA site can switch the phenotype of a bacterial cell (*92*). Interestingly, SOS is the key enzyme involved in bimodal switching from positive to negative selection in maturing thymocytes (*28, 63*), and rare high activity states could play a role in threshold crossing, leading to robust feed-forward activation and cell fate selection.

In conclusion, we developed a fluid SLB-based membrane platform to study Ras activation by SOS at single molecule resolution. We found a wide distribution of long-lived (>100s) dynamic functional states of processive Ras-SOS complexes on lipid membranes. In the functionally competent Ras-tethered state, N-terminal Histone fold, DH and PH domains allosterically autoinhibit SOS-HDPC by suppressing fluctuations to high-activity states. Both N-terminal domains and nucleotide state of Ras changes the functional dynamics of the allosteric and catalytic sites. A Noonan syndrome R552G mutation retains full allosteric autoinhibition in processive catalysis, has lost sensitivity to Ras nucleotide state and membrane PIP_2 lipids in allosteric regulation of specific activity relative to wt SOS-HDPC, but has gained increased activation by Ras-GTP and PIP_2 lipids in terms of membrane recruitment.

4.4 Materials and methods

4.4.1 Chemicals and protein preparation

Please refer to chapter 3 for details in common chemicals. SOS-HDPC (residues 1–1049), SOScat (residues 566–1049) and SOScat-cyslite (SOScat-C838A, C635A, C980S, E716C) derived from human SOS1 were expressed and purified as described (*25-27, 93*). Constructs with point mutant(s) were generated using the Quikchange site-directed mutagenesis kit (Stratagene) and confirmed by DNA sequencing. Ras(C181,C118S) (residues 1–181) was expressed and purified as described (*26, 27*). MS analysis confirmed the identity of the proteins.

Fluorescently labeled SOScat-cyslite was prepared by reacting with 10-fold excess of Atto647N-maleimide for 2.5hrs at 23°C. After labeling, 2 consecutive runs of PD-10 column (GE Healthcare, Pittsburgh, PA) were used to purify labeled SOScat-cyslite from unreacted dye. Degree of labeling was measured by UV/VIS spectroscopy (NanoDrop 2000, Thermo Scientific) and calculated to be more than 90 %.

Patterned substrates preparation and cleaning

Details of substrates preparation and cleaning can be found in section 3.4 of this dissertation.

4.4.2 Optical microscopy

Epifluorescence and total internal reflection fluorescence (TIRF) images were acquired on a Nikon Eclipse Ti inverted microscope with a 100× 1.49 NA oil immersion TIRF objective and an Andor iXon EMCCD camera. A mercury arc lamp was used for epifluorescence illumination. 488 nm (Sapphire HP; Coherent Inc., Santa Clara, CA) and 647 nm (RCL-050-640; Crystalaser, Reno, NV) laser lines were used for TIRF imaging. Bandpass emission filters were HQ515/30 and ET630/75 (Chroma Technology Corp., Bellows Falls, VT), respectively. MetaMorph (Molecular Devices Corp., Downington, PA) software was used to control the microscope.

4.4.3 Preparation of SUVs and Ras conjugated SLBs

Lipid compositions are given in molar percent. Chloroform mixtures of Egg-PC, MCC-PE, TR-DHPE and DOPS or PIP_2 were dried in a rotary evaporator (40°C, 10 min) followed by drying under a stream of nitrogen gas (20 min.). For DOPS-containing vesicles, mixtures contained 3% DOPS, 3% MCC-PE, 0.01% TR-DHPE, and the balance consisted of Egg-PC; for PIP_2-containing vesicles, mixtures contained 2% PIP_2, 1% MCC-PE, 0.01% TR-DHPE and the balance consisted of Egg-PC. Dried lipid films were resuspended in degassed phosphate buffered saline (PBS, pH 7.45) using vortexing. SUVs were formed by extrusion 11 times through a 30 nm polycarbonate filter (Millipore) using a hand-held mini-extruder (Avestin). Vesicles were immediately used to form supported lipid bilayers (SLBs).

SLB formation and experiments were performed in FCS2 flow chambers (Bioptechs). Flushing with 3 mL buffer followed all incubation steps. Maleimide-functionalized vesicles (200 µL, 1 mg/mL in PBS) were incubated on the patterned substrate for 30 minutes, followed by 10 min incubation with Casein (200 µL, 2.5 mg/mL in PBS) and 2.5 hrs incubation with Ras(C181, C118S) (200 µL, 1.3 mg/mL in PBS).

Unreacted MCC-PE was quenched by 10 minutes incubation with 2-mercaptoethanol (5 mM in PBS). Samples were then cooled to 4°C in a cold room and washed with 3mL loading buffer (40 mM HEPES-NaOH (pH 7.4), 150 mM NaCl). Native nucleotide was stripped by 20 minutes incubation with EDTA (50 mM in loading buffer), followed by flushing with loading buffer and over night (ON) incubation with fluorescent nucleotide (10 uM of EDA-GDP-Atto488 or EDA-GppNp-Atto488 in reaction buffer). Reaction buffer is 40 mM HEPES-NaOH (pH 7.4), 100 mM NaCl, 5 mM MgCl2. After ON incubation, Ras-functionalized bilayers loaded with fluorescent nucleotide were brought to room temperature (RT) immediately before use and washed with 3mL reaction buffer under constant flow rate (1mL/min) to remove unbound fluorescent nucleotide.

4.4.4 Sample fluidity and Surface density characterization

To assess the quality of Ras-functionalized supported lipid bilayers fluorescence fluctuation spectroscopy (FFS) of Texas Red-DHPE and fluorescently loaded Ras were performed (Fig. 3-1(B) in chapter 3), using a home-built confocal setup based on a Nikon Eclipse TE2000-E inverted microscope (*50*). Two different analytical methods were applied to analyze measured fluorescence fluctuations. First, time correlation of fluorescence fluctuations were calculated (fluorescence correlation spectroscopy - FCS). Measuring diffusion coefficients of Ras and Texas Red-DHPE with FCS, allowed us to ensure that both species were laterally mobile. Second, photon counting histogram (PCH) analysis allowed us to determine the surface density of Ras accurately. In this way, a calibration curve between widefield epifluorescence intensity and Ras density measured by FFS was established and used for quantification of kinetic traces (Fig. 3-1(C) in chapter 3).

To ensure that Cr corrals were not leaky, fluorescence recovery after photobleaching (FRAP) was performed on corners of a corral arrays (Fig. 3-4 in chapter 3). Recovery outside the array confirms the lateral fluidity of the membrane, while lack of recovery inside the array confirms that Cr lines act as barriers for lateral diffusion.

4.4.5 Single molecule corral assay

To perform single molecule corral experiments SOS constructs (200 µL) were injected as a pulse through the system with a flow rate of 2mL/min. To initiate the SOS-mediated exchange reactions, unlabeled nucleotide (GDP or GTP, 120 µM) in reaction buffer together with 1mM TCEP was provided to stably flow through the sample chamber at a flow rate of 1mL/min for first 4 minutes and 0.2mL/min afterwards. Time-lapse epifluorescence images were collected every 35-40 seconds to measure the reaction kinetics for ~20-25 minutes. In the case of Atto647N-SOScat, TIRF images were taken at the end of the time-lapse recording to show how SOScat diffuses inside the corral.

4.5 Analyze single molecule corral data

4.5.1 Extracting fluorescence decay rates from the corral assay

Epifluorescence images from time-lapse recordings were flattened against reference images acquired outside the corral array, in order to remove intrinsic unevenness caused mainly by the illumination profile. Individual kinetic traces were then extracted using a custom algorithm in Matlab, by measuring the average fluorescence intensity from each identified corral in the image, while avoiding corral grid lines. Kinetic traces were normalized to their own initial maximum intensity value for further analysis.

SOS concentrations were experimentally adjusted so >90% of corrals would be without SOS (Population 2, P2) and <10% of corrals would contain SOS enzyme (Population 1, P1). These populations were identified in images by the intensity difference between the first and last frames in the time-lapse recordings. For P1, the intensity difference is larger due to a combined effect of SOS-mediated turnover, photobleaching, and intrinsic exchange whereas for P2, the difference is smaller due to the lack of SOS-mediated catalysis. The distribution of intensity differences in all corrals in the array was fitted to two Gaussian curves, which correspond to P1 and P2. Because of the existence of slow SOS states, P1 and P2 have an overlapping region, and a threshold of <0.05 % probability of overlap when choosing P1 was used in all analysis.

Each corral has three potential exponential decay channels: (1) SOS turnover, k_{sos}. (2) Photobleaching, k_{PB}. (3) Intrinsic Ras turnover, k_{IT}. For P1, $I(t)_{P1} = I_0*\exp(-(k_{sos}+k_{PB}+k_{IT})*t)$, whereas for P2: $I(t)_{P2} = I_0*\exp(-(k_{PB}+k_{IT})*t)$. To extract the component of the exponential decay attributable to enzyme catalysis, each kinetic trace of P1 was divided by the average kinetic trace of P2: $I(t)_{SOS} = I(t)_{P1} / I(t)_{P2,Avg.} = I_0*\exp(-(k_{sos})*t)$. k_{sos} describes the rate of decay of fluorescence due to SOS turning over a constant reservoir of Ras in the presence of a constant concentration of non-fluorescent nucleotide in solution.

Dividing the individual traces of P1 with the average trace from all P2 in the array gives corrected baseline traces for zero catalytic turnover. Both the intrinsic nucleotide release and the photobleaching decay paths average thousands of Ras in each corral, minimizing stochastic variation. Differences in fluorescence decay rates between empty corrals mainly result from experimental error. The width of the distribution of decay constants from P2 is therefore used to estimate the error associated with the experimental setup.

4.5.2 Extracting molecular kinetic parameters

A nucleotide exchange reaction catalyzed by one SOS enzyme in the corral assay can be described by the following reaction scheme S1:

$$Ras^{*} + SOS \underset{\text{koff}}{\overset{\text{kon}}{\leftrightarrow}} Ras^{*} \cdot \mathrm{SOS} \xrightarrow{\text{kcat}} \mathrm{Ras}^{0} + \mathrm{SOS}$$

$$Ras^{0} + SOS \underset{\text{koff}}{\overset{\text{kon}}{\leftrightarrow}} Ras^{0} \cdot \mathrm{SOS} \xrightarrow{\text{kcat}} \mathrm{Ras}^{0} + \mathrm{SOS}$$

Figure 4-11. Reaction scheme describing SOS-catalyzed nucleotide of Ras.

Where Ras* represents Ras loaded with fluorescent nucleotide, Ras^{0} represents Ras loaded with non-fluorescent nucleotide, kon is the association rate constant, koff is the dissociation rate constant, and kcat is the catalytic rate constant. The total number of Ras (R_{total}) in each corral stays the same and initially all Ras are loaded with fluorescent nucleotide, i.e. $R_{total} = R^{*}_{(t=0)}$.

In the following analysis, we assume SOS-catalyzed exchange does not distinguish between Ras* and Ras^{0}. As a result, the effect of SOS catalyzing Ras^{0} relative to catalyzing Ras* during the reaction will be proportional to the numbers of Ras^{0} and Ras*, respectively.

A single molecule Michaelis-Menten equation has the following form (*75, 94*):

$$\frac{1}{<\tau>} = kcat \times \frac{[S]_0}{K_M + [S]_0}$$

Where $<\tau>$ is the mean waiting time and $1/<\tau>$ can be interpreted as an average reaction rate (*94*), $[S]_0$ is the substrate concentration and $K_M = \frac{k_{off}+k_{cat}}{k_{on}}$. In the assay, $[S]_0 = R_{total}$ in each corral. Since the assay measures the fluorescence decrease per single SOS due to the exchange of Ras* with Ras^{0}, the following equation can be used to describe the system:

$$-\frac{dRas^{*}(t)}{dt} = \frac{1}{<\tau>} = \frac{Ras^{*}(t)}{R_{total}} \times k_{cat} \times \frac{R_{total}}{K_M + R_{total}}$$

$$-\frac{dRas^{*}(t)}{dt} = Ras^{*}(t) \times k_{cat} \times \frac{1}{K_M + R_{total}}$$

$$Ras^{*}{}_{(t)} = Ras^{*}{}_{0} \times e^{-(k_{cat} \times \frac{1}{K_M + R_{total}} \times t)}$$

$$= Ras^{*}{}_{0} \times e^{-(k_{app} \times t)} \qquad \text{with } k_{app} = k_{cat} \times \frac{1}{K_M + R_{total}}$$

Where $Ras^{*}{}_{(t)}$ and $Ras^{*}{}_{0}$ represent number of Ras* at time t and time 0, respectively, and k_{app} is the rate constant for fluorescence decay (per SOS enzyme). To calculate the turnover number TN=ΔRas/Δt of products catalyzed by one SOS per second we can use the expansion:

$$\Delta Ras = Ras^{*}{}_{0} - Ras^{*}{}_{(t)}$$

$$= Ras^*{}_0 \times (1 - (1 + (-k_{app} \times t) + \frac{(-k_{app} \times t)^2}{2!} + \cdots)$$

$$\approx Ras^*{}_0 \times k_{app} \times t \qquad \text{when } k_{app} \text{ is small}$$

For all analysis and discussion, this equation was used to convert apparent rate constants to TN by TN=ΔRas/t $=k_{app}$ x Ras^*_0.

This is the general result for k_{app} for a SOS mechanism that can be described by the MM equation, and for the turnover number TN when k_{app} is small. The measured k_{app} values are in the range of 10^{-4} s^{-1}, justifying omitting the higher order terms in the expansion.

The physical interpretation of k_{app} depends on whether Ras density is saturating. In the limiting case where substrate concentration is low, K_M+R_{total} ~ K_M and kapp ~ kcat/K_M. Conversely, when R_{total} is saturating and the enzyme k_{cat} becomes rate limiting, K_M+R_{total} ~ R_{total} and k_{app} ~ k_{cat}/ R_{total}. Our results indicate that for all SOS constructs and conditions probed, the rate dependence on R_{total} is small compared to intrinsic scattering due to variation in k_{cat} and/or K_M (Fig. 4-4).

4.5.3 Quantification of enzyme kinetics

Apparent rates of enzymatic turnover were quantified using an unbiased and automated approach. Single-enzyme turnover traces were generally characterized by the presence of a number of well-defined kinetic states, i.e., the enzyme exhibits a characteristic rate of catalysis for a finite time interval and then switches to work at another rate. Evident transitions between such activity states were frequent and, naturally, the first step in inferring rates of catalysis from the data was to localize the different states within each trace.

This was achieved using the change point algorithm developed by Ensign and Pande (*95*). The change point algorithm was originally designed for the purpose of identifying transitions in time-series of a stochastic variable spontaneously fluctuating between distinct levels. Change point analysis of the catalysis data was performed after recasting the turnover traces in terms of the observed local rate of catalysis (defined as the change in fluorescent intensity in between two measured time-points weighted with the time lapsed). A Bayes factor of 3, generally accepted to reflect ”substantial evidence”, was applied as a criterion in change point identification (*95*). Having localized all statistically significant change points, the apparent turnover rate was obtained for each state as the slope of the least-square fit of the turnover trace to a straight line (Fig. 4-5(A)). The data treatment scheme was implemented in Igor Pro ver. 6.22A (WaveMetrics, Lake Oswego, Oregon, U.S.A.) and operated via a graphical user interface, allowing inspection of the consistency of the identified states and fitted kinetics.

4.6 Stochastic simulation of Ras/SOS reaction network

A model was constructed to simulate the interaction of membrane-bound Ras with SOS in the corral assay. We use a convention where "*Ras·SOS"* indicates Ras bound in the allosteric site, "*SOS·Ras"* indicates Ras bound in the catalytic site, and "*Ras·SOS·Ras*" indicates Ras in both allosteric and catalytic sites. *Ras** represents a Ras loaded with fluorescent nucleotide whereas Ras^0 is a Ras with non-fluorescent nucleotide. Our model assumes that SOS is able to switch the binding partners at both allosteric and catalytic sites but only catalyzes nucleotide exchange at the catalytic site. Once a SOS disengages from both sites it will not be able to bind any Ras again, to simulate the case in the corral assay where a SOS unbinds from surface and is flushed away. Our model contains the following reactions scheme:

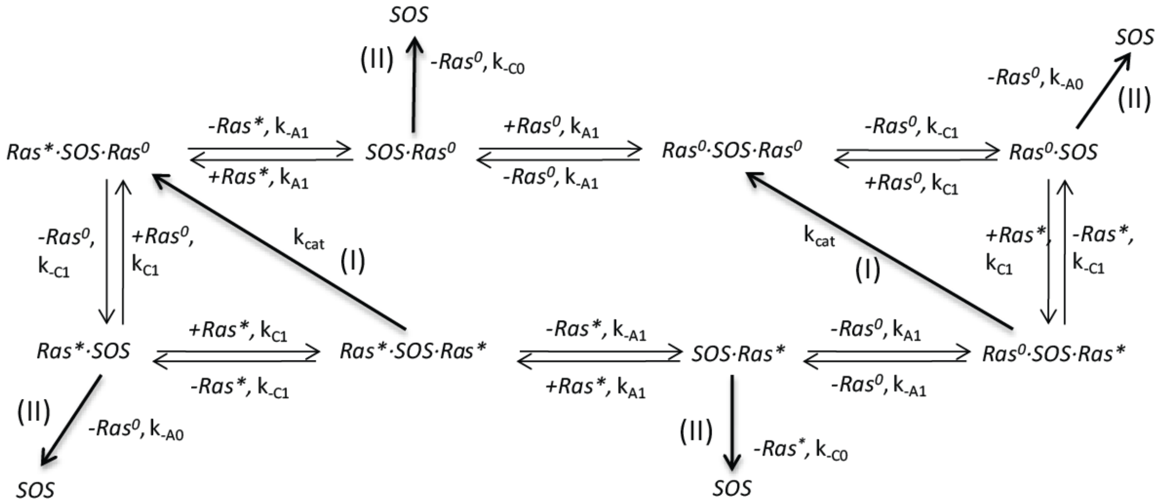

Figure 4-12. Simplest-case reaction network for the reconstituted Ras-SOS system. Path (I) corresponds to a turnover and (II) represents the desorption of SOS from the membrane.

Where the rate constants represent (*26*):

k_{-A0} = unbinding from allosteric site (empty catalytic site)
k_{-C0} = unbinding from catalytic site (empty allosteric site)
k_{A1} = binding to allosteric site (filled catalytic site)
k_{-A1} = unbinding from allosteric site (filled catalytic site)
k_{C1} = binding to catalytic site (filled allosteric site)
k_{-C1} = unbinding from catalytic site (empty allosteric site)
k_{cat} = nucleotide exchange rate constant with allosteric Ras bound

The rate constants used in the simulation were derived and chosen in order to qualitatively describe the system (*26*), (*28*).

In this reaction scheme, only channel (I) leads to a nucleotide exchange reaction. On the other hand, channel (II) describes the case where a SOS unbinds from the surface. A stochastic simulation was performed based on the Gillespie algorithm for calculating reaction kinetics (*96*). In this method, the kinetic rate constants are replaced by a set of transition probabilities, p, which define the probability that a single molecule undergoes a conversion from one state to another (*96*), (*97*).

To generate a trajectory from stochastic simulation, we assume each reaction starts at the upper left corner ($Ras^{*}\cdot SOS\cdot Ras^{0}$) in the reaction scheme (Fig. 4-12) and determine the reaction direction by evaluating the transition probability based on the rate constants (listed below). We assume the reaction starts with all Ras bound to fluorescent nucleotide (Ras*) and its initial value can be obtained directly from experiment. A Ras* density of 600 Ras/μm^2 was used in the simulation. A single trajectory was recorded using a time step of 0.06 ms for 500 seconds. We then keep track of the positions of SOS in the reaction scheme and update it after each time step. When the simulation goes through channel (I), a nucleotide exchange event is recorded and number of Ras* and Ras^0 will be updated. Specifically, number of Ras* is decreased by 1 and number of Ras^0 is increased by 1. On the other hand, once SOS goes through channel (II) in the reaction scheme, it will stay as (*S*) throughout the simulation and no more exchange would occur since it represents a SOS unbinding event.

Under this condition, one trajectory of Ras* decay over time represents the enzymatic activity observed for a single SOS catalyzing nucleotide exchange in a corral. A total of 500 stochastic simulations were performed and allowed us to extract the corresponding ensemble distribution kinetics and make a comparison to the experimental data.

Rate constants used in the stochastic simulation (details of unit conversion can be found in (*26*)):

$k_{-A0} = 0.008\ s^{-1}$;
$k_{A1} = 12000\ s^{-1}$;
$k_{-A1} = 6\ s^{-1}$;
$k_{-C0} = 0.008\ s^{-1}$;
$k_{C1} = 6000\ s^{-1}$;
$k_{-C1} = 5\ s^{-1}$;
$k_{cat} = 1.5\ s^{-1}$

Chapter 5 Current study on RasGRP1-catalyzed Ras activation and future work

5.1 Introduction

Ras is a membrane-associated small GTPase which plays a pivotal role in mediating various important signaling cascades. Two families of proteins, guanine nucleotide exchange factors (GEFs) and GTPase activating proteins (GAPs), are involved in maintaining proper level of Ras signaling in cells. GEFs turn on Ras signaling by catalyzing Ras from GDP to GTP bound whereas GAPs terminate signaling by catalyzing the hydrolysis of bound GTP to GDP. Many GEFs and GAPs are multi-domain proteins with their enzymatic activity being autoinhibited as part of its regulation (*17, 19*). To be fully activated at the membrane, GEFs and GAPs respond to various biochemical inputs and undergo consequent structural changes to relieve the autoinhibition. Son of Sevenless (SOS) is one of the best characterized mammalian GEFs in terms of its structure and regulatory mechanisms imposed by intra-molecular domain interactions (*23-25, 27*). It has been shown that cooperative actions involving membrane interactions between domains and lipids/proteins are necessary for the activation of SOS (*26, 27, 29*).

In addition to ubiquitously expressed SOS, both T and B lymphocytes contain a specifically expressed GEF, Ras guanyl nucleotide-releasing protein (RasGRP1) (*38, 98*). RasGRP1 and SOS activities are non-redundant in immune cells, and the combined action of the two proteins leads to complex patterns of Ras activation (*99*). For example, Roose and colleagues revealed a mechanism by which RasGRP1 generates Ras-GTP, which then enhances SOS activity by binding to an allosteric site on SOS. This creates a positive feedback loop for Ras activation *in vivo* (T- and B-cell lines) (*63*). Later, Das and colleagues combined *in silico* simulations and *in vivo* studies to further demonstrate the importance of the interplay between RasGRP1 and SOS in generating more efficient digital signaling output in lymphocytes (*28*). On the other hand, a recent study by Warnecke and Poltorak *et al.* on primary human T cells indicated that RasGRP1 and SOS mediate Ras signaling differently conditional of upstream stimuli, specifically RasGRP1 triggers T cell receptor (TCR) mediated extracellular signal-regulated kinases (ERK) activation while SOS is involved in IL2-mediated ERK activation. Recently, it has been suggested that Ras and downstream ERK activation at different stages of thymocyte development shows different RasGEFs-dependency (*99*), therefore providing a potential mechanism to account for the observed discrepancy in the aforementioned studies. However, more experiments are required to test the hypothesis.

Like SOS, RasGRP1 contains several domains. First discovered in 1998, RasGRP1 was found to contain the Ras exchanger motif (REM) and Cdc25 domain, both of which are also found in SOS, as the catalytic unit in its N-terminal (*35*). Following the Cdc25 domain, an atypical pair of EF hands which has shorter linker between two calcium binding loops was identified (*100*). In addition, the C1 domain binds to diacylglycerol (DAG) or phorbol 12-myristate 13-acetate (PMA) and is located C-terminal to EF hands (*36, 37, 101*). Among these domains, the C1 domain is of particular interests because it potentially links Ras to DAG related signaling pathways. In fact, DAG has been shown to affect the function of RasGRP1 either through direct membrane recruitment (*38*) or by protein kinase C (PKC) mediated phosphorylation (*102*). On the other hand, the functional role of EF hands is less clear. Only one of the EF hands binds calcium *in vitro* (*35*). Later studies demonstrated that the EF hands were not involved in the transforming activity of RasGRP1 (*101*), nor did it play significant role in conferring calcium dependence to PMA/C1 binding interaction *in vitro* (*103*). A recent study in B cell lines suggested that one of the EF hands, EF1, is required for receptor-induced membrane localization of RasGRP1, but in a calcium independent manner (*104*).

In addition to C1 domain, plasma membrane targeting (PT) and suppressor of PT (SuPT) domains located in the C-terminal were identified to participate in membrane localization of RasGRP1 (*105*). Later, Fuller and colleagues confirmed the functional role of the C-terminal tail domain (which includes both PT and SuPT domains) in mediating membrane localization and further established the importance of the tail domain in T cell development and activation *in vivo* (*106*). In addition, a recent structural study by Iwig and colleagues showed that ~40 residues in the C-terminal form a parallel coiled coil dimeric interface, implying that the full length protein might be dimeric (Jeff Iwig *et al.*, University of California Berkeley, unpublished data).

The structure of RasGRP1 suggests that multiple inputs and interactions from the membrane are required to fully activate RasGRP1. It is thus desired to study the Ras-RasGRP1 interaction at the membrane surface. In this on-going project, we aim to understand how RasGRP1 catalyzes nucleotide exchange on the membrane. Specifically we would like to independently probe the membrane recruitment and enzymatic activity of RasGRP1 in reconstituted supported membrane. A RasGRP1 construct containing REM, Cdc25, EF hands and C1 domains (referred as RGcec from hereon; Fig. 5-1(A)) was used in the current study. Direct measurements of the effect of DAG on the membrane localization of RasGRP1 based on single molecule imaging were performed at Ras functionalized supported bilayer. Interestingly, we find that DAG only weakly affects the on rate and specific activity of RasGRP1, indicating that it functions primarily by increasing the residence time of RasGRP1 at the membrane, where it encounters Ras.

5.2 Preliminary Results

5.2.1 DAG lipid increases membrane recruitment of RGcec

The biological role of RasGRP1 is to catalyze the nucleotide exchange of membrane anchored Ras. We reconstituted this protein-protein reaction on the supported lipid bilayers as it recapitulates the two dimensional geometry and allows easy access to various microscope techniques such as epi-fluorescence and total internal reflection fluorescence (TIRF) microscopy. H-Ras functionalized supported bilayers were prepared as described in previous chapters (section 3.4 and 4.4 of this dissertation). In short, H-Ras was tethered to the bilayer through the coupling reaction between cysteine 181 of H-Ras and maleimide group on lipids. H-Ras was then loaded with fluorescent nucleotide to allow the visualization of H-Ras and consequent nucleotide exchange reaction. Two dimensional

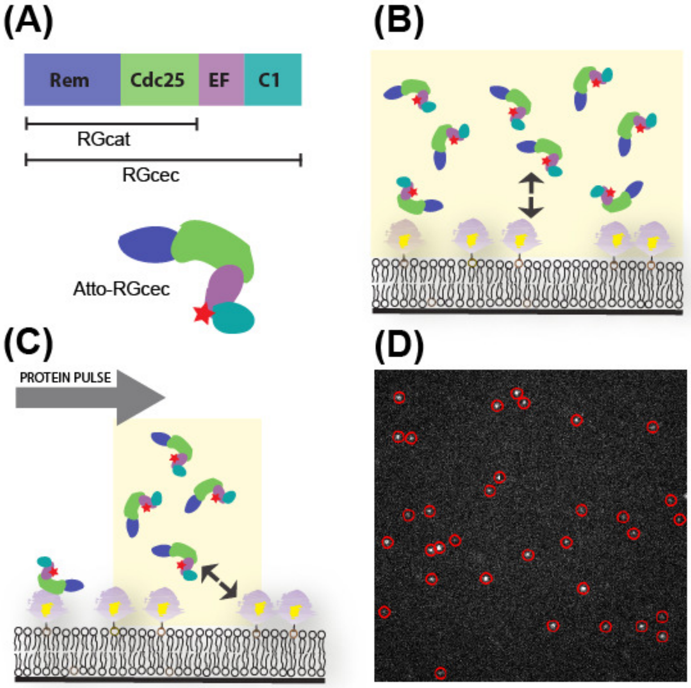

Figure 5-1. Reconstituted supported bilayer assays to study Ras activation by RasGRP1. (A) The domain organization of the RasGRP1 construct used in this study. The protein is labeled with Atto647N fluorophore (represented as a red star). Cartoon representations of single molecule supported bilayer assays for (B) on-rate and (C) recruitment measurements. For on rate measurements, a low concentration of Atto-RGcec (50 pM) was incubated with bilayer samples, whereas 1 nM Atto-RGcec was injected as a pulse in the recruitment assay. In both cases, a series of TIRF images were acquired to monitor the membrane localization of Atto-RGcec. (D) A representative TIRF image of Atto-RGcec on the bilayer. Red circle marks the position of individual particles after data analysis.

fluidity of the samples was confirmed by fluorescence recovery after photobleaching (FRAP) measurement. In addition to epi-fluorescence microscopy, TIRF microscopy was used throughout this chapter to probe the number and diffusion of labeled RGcec (referred as Atto-RGcec from hereon; Fig. 5-1(A)) at the membrane surface. Two kinds of bilayer assays, the single molecule on-rate and diffusion probing assay and protein pulse assay, will be used in this study (Fig. 5-1(B) and (C); for assay details, please see section 5.4 and appendix 1 of this dissertation). Both assays rely on the direct imaging and counting of proteins binding to the membrane (Fig. 5-1(D)).

We first performed a vesicle-based functional assay (*26*). Small unilamellar vesicles (SUVs) containing fluorescent nucleotide loaded Ras were prepared and mixed with 5uM of RGcec and unlabeled nucleotide to start the exchange reaction. Figure 5-2(A) shows representative intensity traces from RGcec-catalyzed nucleotide exchange reactions on SUVs with (red trace) and without (black trace) DAG lipids, respectively. The data showed ~ 50 fold increase in apparent activity when DAG was included in the SUVs (Fig. 5-2(A), inset). However, the vesicle assay cannot address whether the increased activity is purely due to more protein recruitment (faster on rate/longer residence time) or accelerated specific activity, or perhaps both. In signaling networks, it has been shown that changes in the amplitude or duration of signaling can lead to distinct functional outcomes (*107, 108*). In the case of RasGRP1, a longer residence time due to the interaction between C1 domain and DAG would potentially prolong the signaling duration, whereas enhanced enzymatic activity or faster on rate would result in higher peak amplitude.

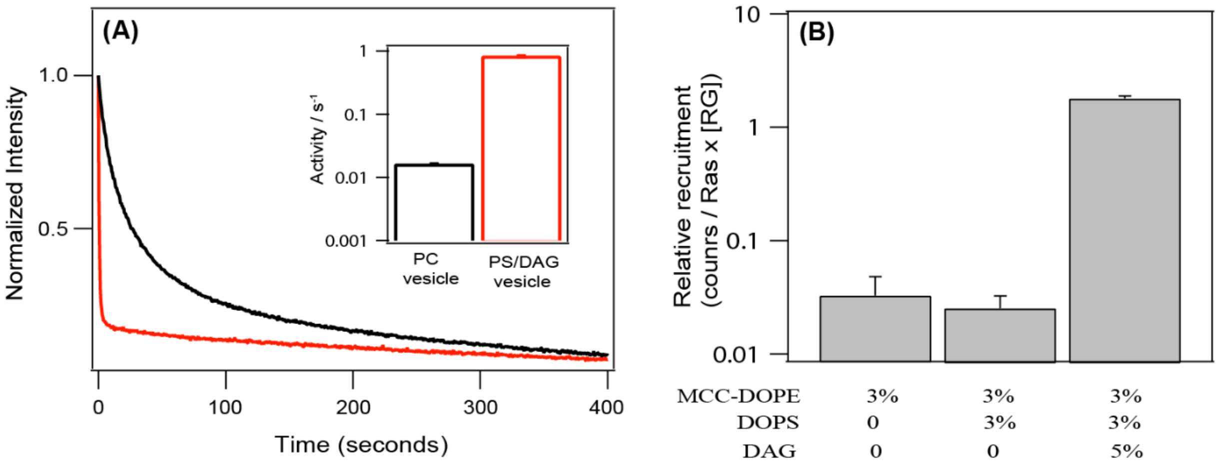

Figure 5-2. DAG lipid increases the membrane localization of RGcec. (A) Representative intensity traces of fluorescent nucleotide released from Ras upon RGcec catalysis measured in the vesicle assay. Inset: ~50 fold rate enhancement was observed in the DAG vesicles. (B) Recruitment probability of labeled RGcec based on protein pulse assay (see materials and methods section for details) shows DAG greatly enhance the surface engagement of RGcec. Interestingly, negatively charged DOPS lipid has no effect on the membrane localization.

To determine whether DAG, through the interaction with C1 domain of RGcec, directly modulates enzymatic activity or simply affects membrane recruitment, bilayers with and without DAG were prepared and used in the protein pulse assay. This assay allows the quantification of membrane-bound Atto-RGcec by single molecule counting upon the injection of protein pulse. The data showed that more RGcec (~ 50 fold) were recruited on the Ras bilayer where DAG was also included (Fig. 5-2(B)). Interesting, the fold increase in protein recruitment is consistent with the rate enhancement observed in the vesicle assay, suggesting DAG regulates RasGRP1's function mainly through recruitment but not its enzymatic activity (see section 5.2.4 for the study on specific activity). A control experiment performed on bilayers with neither 1,2-dioleoyl-*sn*-glycero-3-phospho-L-serine **(**DOPS, a negatively charge lipid) nor DAG further confirmed that the enhancement is DAG-specific (Fig. 5-2(B)).

5.2.2 DAG minimally affects the on rate of RGcec

Since more efficient protein localization can be a result of (1) faster on rate, (2) slower off rate (residence time) and (3) a combination of (1) and (2), we utilized a bilayer assay that is able to directly measure the on rate. In short, a series of TIRF images were acquired (frame rate = 32 Hz) during 50pM Atto-RGcec incubation under different conditions. By analyzing the number of bound proteins as a function of time for each condition, the corresponding on rate can be obtained (Fig. 5-3). Figure 5-3(A) shows a plot of accumulated counts of bound Atto-RGcec as a function of incubation time for samples with (green trace) and without (red trace) Ras, respectively. The corresponding on rate can be obtained by fitting individual traces from such plot. Figure 5-3(B) shows the on rate for

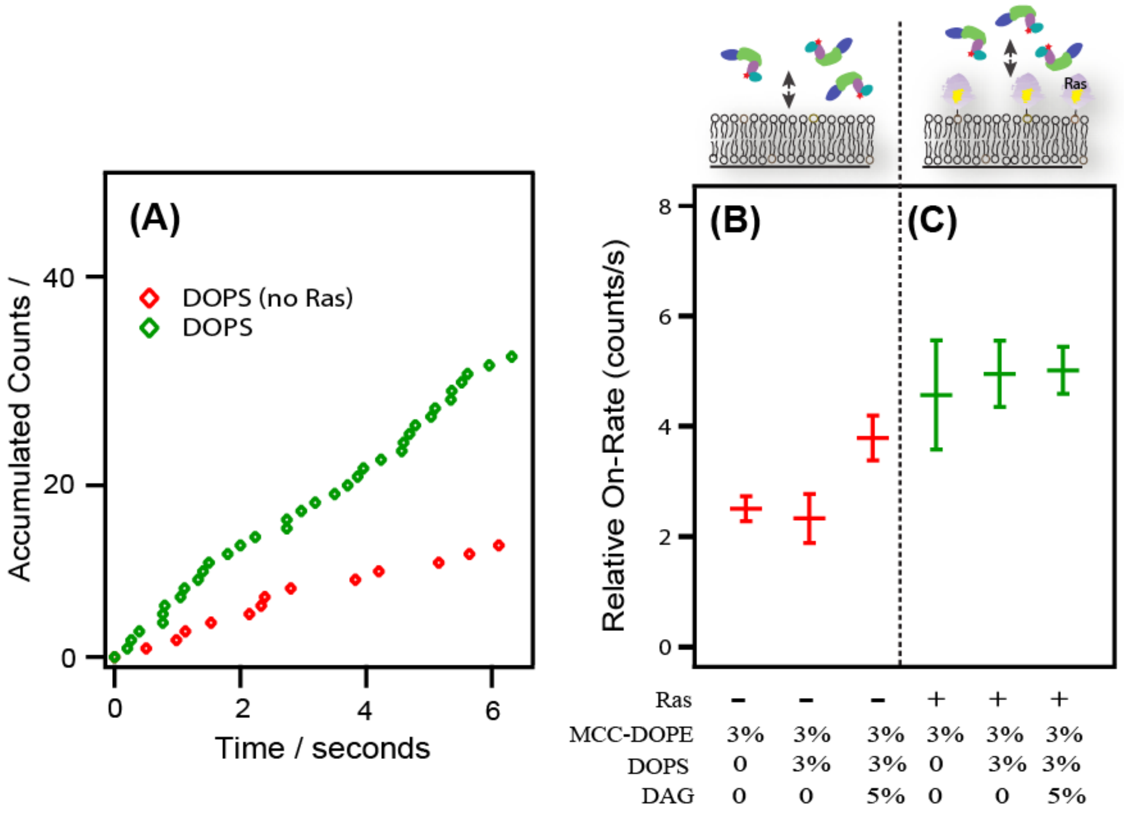

Figure 5-3. **The on rate measurement and the effect of DAG lipid.** (A) Representative traces from single molecule on rate measurements are shown for 3%MCC-DOPE and 5%DOPS samples with (green) and without (red) Ras functionalization, respectively. From the slope of individual traces one can obtain the on-rate of labeled RGcec to the surface. (B) Without Ras on the surface, DAG specifically increases the surface recruitment of labeled RGcec. (C) Interestingly, in the presence of Ras DAG does not affect the on rate of RasGRP1. The data shown in (B) and (C) were averaged over 20 measurements and 2 individual samples for each condition.

the bilayer without Ras. The data indicate that DAG increases the on rate by ~ 1.6 fold when compared to bilayers without DAG.

Surprisingly, DAG seems to have no effect of the on rate in the presence of Ras (Fig. 5-3(C)). All Ras samples have similar on rates, which were slightly higher than bilayers without Ras (Fig. 5-3(B)). One possible explanation is that at the Ras densities we worked with (~hundreds of Ras/μm^2), the interaction between Ras and the Cdc25 domain dictates the observed on rate. One can examine whether this is the case by measuring the on rate as a function of Ras density. Another possibility is that RGcec cannot bind DAG and Ras simultaneously while on the membrane. Nevertheless, the result clearly demonstrated that DAG does not significantly increase the on rate of RGcec to the Ras membrane, as was the case in the samples without Ras. Based on this observation and the previous discussion in section 5.2.1, we speculate that DAG, through the interaction with C1 domain, regulates the function of RGcec in two ways: (1) in an area without Ras, DAG increases the on rate of RGcec to the membrane; (2) in the presence of Ras, the data indicated that DAG does not enhance the on rate of RGcec. Our data suggest that DAG increases nucleotide exchange activity by extending the membrane residence time of RGcec. More experiments are required to confirm this hypothesis.

5.2.3 Diffusion of Atto-RGcec at the membrane

Two dimensional diffusion is another important physical parameter in membrane related reactions. We found that even though the difference in the on rate between samples with and without Ras is only ~ 2 fold (Fig. 5-3(B) and (C)), the diffusion behavior of Atto-RGcec is drastically different (Fig. 5-4).

In chapter 2, we quantified both lipids and Ras diffusions. It was found that lipids usually diffuses around 3μm^2/s whereas Ras exists as two populations and has diffusion coefficient of ~3 μm^2/s and ~0.8 μm^2/s, respectively.

For the diffusion of Atto-RGcec, the step-size distribution and concatenated tracks collected from the single molecule imaging (frame rate = 32 Hz) showed that Atto-RGcec diffuses faster on bilayers without Ras (blue traces; Fig. 5-4(A) and (B)). The preliminary diffusion analysis (Fig. 5-7; please see section 5.4 for details in the diffusion analysis) suggested that ~85% of Atto-RGcec diffuses at 2.4 μm^2/s on bilayers without Ras whereas ~51% and ~36% of Atto-RGcec diffuses at 0.15 μm^2/s and 1.4 μm^2/s on Ras bilayers, respectively.

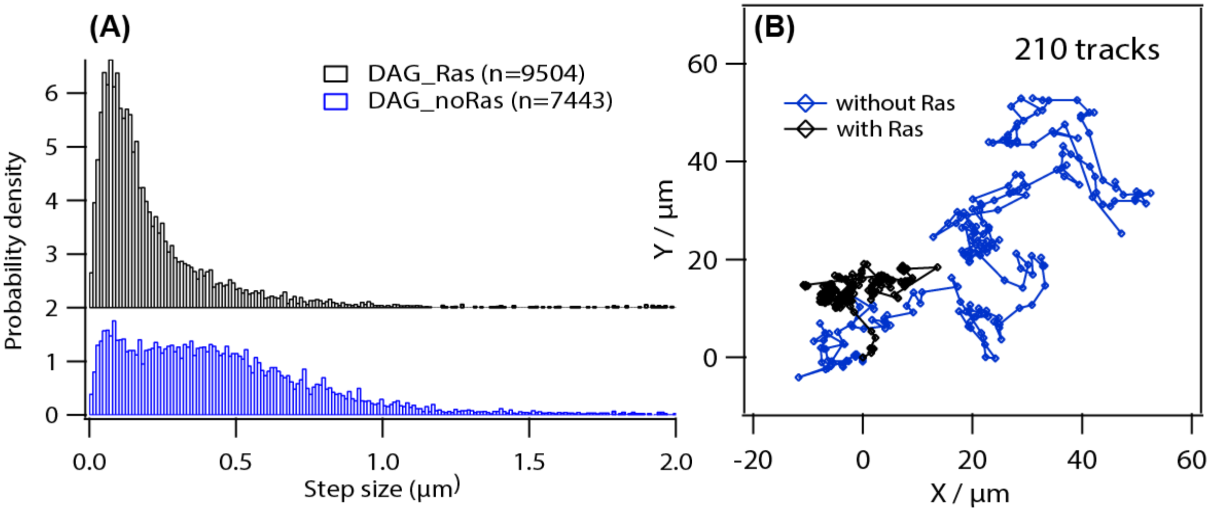

Figure 5-4. **Ras significantly slows down two dimensional diffusion of Atto-RGcec.** (A) The step-size distribution collected from single molecule analysis on DAG bilayer samples with (black trace) and without (blue trace) Ras functionalization. The time interval for step-size shown here is 31 msec. (B) The representative concatenated tracks. In the case of Ras bilayers (black trace), usually localized diffusion was observed. For step-size distribution, data was from 2 independent samples (total of 20 measurements). The concatenated tracks, on the other hand, was connected from a single measurement (300 frames).

This result is informative because it suggested that majority of Atto-RGcec engaged Ras on the membrane and hence diffused considerable slower when compared to their counter partners on bilayer without Ras. It is also intriguing to see that ~51% of Atto-RGcec diffuses at 0.15 $\mu m^2/s$ on Ras bilayer, which is close to the diffusion of slower Ras species (0.8 $\mu m^2/s$) observed in chapter 2, raising the hypothesis that RGcec specifically binds to slower diffusing Ras. In order to confirm the hypothesis, however, more thorough diffusion analysis and control experiments such as simultaneously tracking of RGcec and lipid/Ras diffusion will be required.

5.2.4 DAG lipid does not alter specific activity of RGcec

Even though previous data suggested that DAG regulates the function of RGcec mainly through membrane localization, it is not known, nevertheless, whether DAG also modulates enzymatic activity at single molecule level. To probe the specific activity from individual proteins, single molecule corral assay introduced in previous chapter was used. A series of Ras samples on micro-patterned substrates with various lipid compositions were prepared as described in chapter 4 (please see section 3.4 and 4.4 of this dissertation for details). Representative epifluorescence images showed that a small percentage of corrals experienced RGcec-mediated nucleotide exchange and appeared darker (Fig. 5-5(A) and (B)). By measuring the fluorescent intensity during the exchange reaction, one can study the kinetics from a single enzyme (please see section 4.4 and 4.5 of this dissertation for details in data analysis). We performed RGcec-catalyzed reactions on bilayers (1) with neither DOPS nor DAG, (2) with only DOPS and (3) with both DOPS and DAG. The data

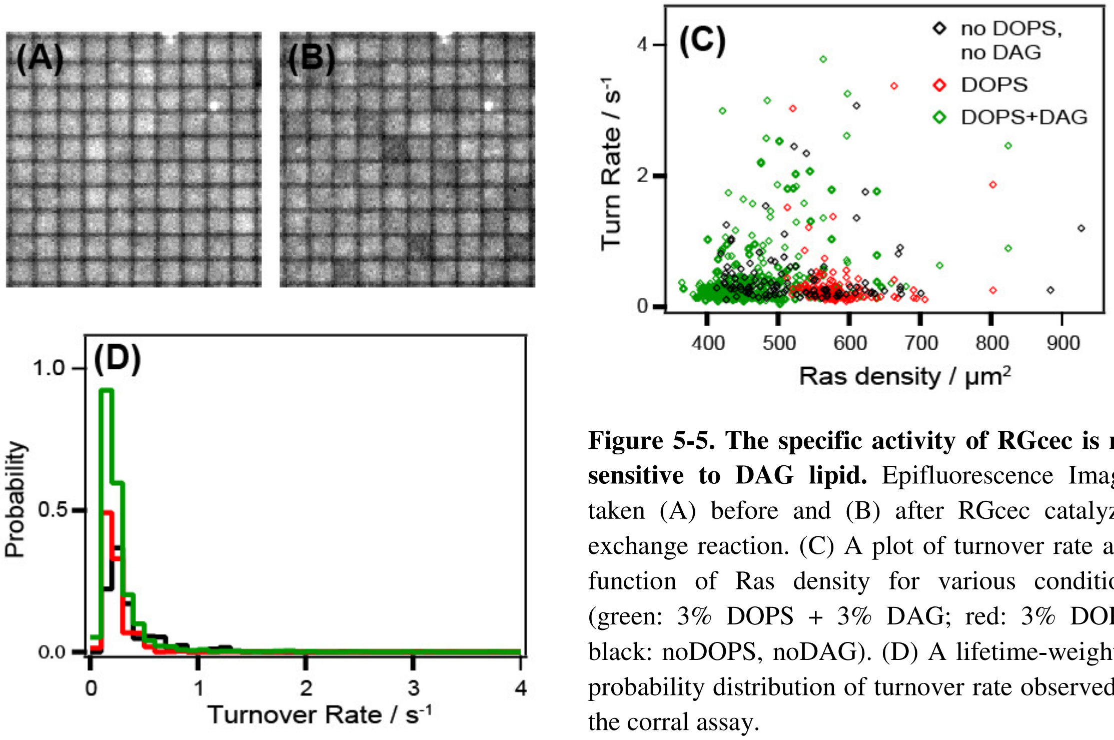

Figure 5-5. The specific activity of RGcec is not sensitive to DAG lipid. Epifluorescence Images taken (A) before and (B) after RGcec catalyzed exchange reaction. (C) A plot of turnover rate as a function of Ras density for various conditions (green: 3% DOPS + 3% DAG; red: 3% DOPS; black: noDOPS, noDAG). (D) A lifetime-weighted probability distribution of turnover rate observed in the corral assay.

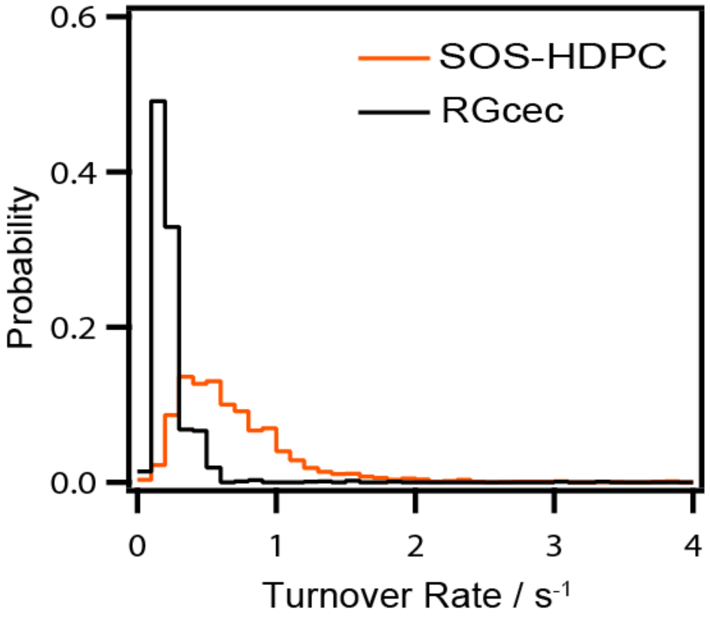

Figure 5-6. RGcec has slower specific activity in catalyzing nucleotide exchange. A comparison of the specific activity measured by the single molecule corral assay for SOS-HDPC (orange) and RGcec (black) on 3% DOPS Ras samples.

indicates that there is no detectable difference in the specific activity of RGcec under these conditions (Fig. 5-5(C) and (D)), thereby supporting the idea that the main function of DAG is to increase the membrane localization instead of modulating the specific activity of RGcec.

5.2.5 RGcec catalyzes the nucleotide exchange slower than SOS-HDPC

The corral assay also allows the comparison of the specific activity between SOS constructs and RGcec. Figure 5-6 shows the rate histogram of SOS-HDPC and RGcec (for SOS-HDPC data, please see chapter 4 for details). Interestingly, the data suggests that RGcec, under the same experimental condition, catalyzes nucleotide exchange at a slower rate. Even though both SOS-HDPC and RGcec used in this study is not full length protein, the data still provides useful information to help understand the interplay between the two GEFs in activating Ras in lymphocytes. As pointed out in previous chapter, SOS contains a pleckstrin homology (PH) domain that binds to phosphatidylinositol 4,5-bisphoshate (PIP_2) (*26*), therefore providing a potential mechanism to link Ras and PIP_2 related signaling pathways. Based on the observation in this chapter that DAG efficiently increases the recruitment of RasGRP1, it would be very interesting to see if PIP_2, through the interaction with PH domain, also enhances the membrane localization of SOS. The fact that RasGRP1 and SOS, through the lipid interacting domains, responses to different signaling lipids also provides possible mechanisms by which Ras can be activated by either RasGRP1 or SOS, depending on the local lipid environment.

5.3 Discussion and future work

Based on the current data from RGcec, the emerging picture of how DAG regulates RasGRP1 function can be understood as follows. First, in a region without Ras, DAG slightly increases (~1.6 fold) the on rate of RasGRP1, thereby allow RasGRP1 to bind transiently to membrane and perhaps search for nearby Ras with reasonable lateral mobility ($D \sim 3\ \mu m^2/s$ on model membrane). On the other hand, when RasGRP1 is recruited directly via Ras on the membrane, DAG seems to have no effect on the on rate. We hypothesize that under this situation, DAG increases the membrane residence time of RasGRP1, therefore allowing RasGRP1 to activate more Ras. Experiments allowing the measurement of residence time are necessary and currently being performed to test this hypothesis.

In addition to RasGRP1, C1 domains are found in other signaling proteins such as protein kinase C (PKC), chimaerins, diacylglycerol kinases (DGKs), etc. Our current study suggested that DAG, through the interaction with C1 domain, increases the membrane localization of RasGRP1. It would be interesting to see if similar regulatory mechanism is involved in other proteins containing the C1 domain.

Even though this study provides a possible mechanism by which the interaction between DAG and the C1 domain can regulate the function of RasGRP1, there are still unaddressed questions and many concerned with the functional role of individual domains. For example, what is the functional role of the EF hands and does Ca^{2+} play any role is RasGRP1 activation and regulation? What is the functional unit of RasGRP1 in catalyzing nucleotide exchange? Does RasGRP1 prefer binding to slower diffusing Ras or does RasGRP1 form a dimer on the membrane itself? In addition, it was indicated that the tail domain of RasGRP1, presumably via PT domain, is also involved in membrane localization. What is its lipid specificity and sensitivity? How does the C1 and tail domain together regulate membrane localization of RasGRP1? Experimentally addressing these questions is essential in order to get a better understanding of Ras activation by RasGRP1.

5.4 Materials and Methods

5.4.1 Chemicals and proteins

All chemicals including lipids and various reagents were purchased from suppliers listed in previous chapters (section 3.4 and 4.4).

RGcec and RGcec-cyslite (RGcec-C80S, C122S, C237S, C251S, C302S, C347S, C507S and D349C) was expressed in *E. coli* BL21(DE3) cells grown at 37 ºC in Terrific Broth with 50 µg/ml kanamycin grown to an OD of ~1.0. Cells were then induced with 1mM IPTG at 15 ºC for 14-18 hrs. The growth media was supplemented with 30 µM $ZnCl_2$. Cell pellets were resuspended in Buffer A (25 mM Tris (pH 8.0), 500 mM NaCl, 10% glycerol, 20 mM imidazole and 5 mM beta-mercaptoethanol (βME)) and frozen at -80 ºC. All purification steps were carried out at 4 ºC using columns from GE Healthcare (Pittsburg, PA). Cells were lysed with a cell disrupter with 5 mM βME, 200 µM AEBSF, 5 µM leupeptin and 500 µM benzamidine. Clarified lysates were applied to a 5 ml HisTrap FF affinity column equilibrated in Buffer A. The column was then washed with 100 ml Buffer A, and the protein was eluted in Buffer A with 500 mM imidazole. RasGRP1 was immediately desalted in Buffer B (25 mM Tris (pH 8.5), 100 mM NaCl, 10% glycerol and 1 mM TCEP) using a HiPrep 26/10 desalting column. The 6xHis-Sumo tag was removed by addition of ULP1 protease and incubation at 4 ºC for 14-18 hrs. The protease and tag were removed by a second pass over a HisTrap FF column in Buffer A. The flow-through and wash fractions were concentrated to 2 ml and further purified on a Superdex 26/60 column equilibrated in Buffer B. Fractions containing pure protein were concentrated and frozen at -80 ºC until use. Purification of $\text{RasGRP1}^{\text{CEC}}$ yielded ~1 mg of protein per liter of cells. Constructs with point mutants (RGcec-cyslite) was generated using the Quikchange site-directed mutagenesis kit (Stratagene) and confirmed by DNA sequencing.

Fluorescently labeled RGcec-cyslite (Atto-RGcec) was prepared and purified based on the procedures described in chapter 3 (section 4.4). The degree of labeling was measured by UV/VIS spectroscopy (NanoDrop 2000, Thermo Scientific) and calculated to be 80%.

Preparation of Ras functionalized supported lipid membranes

Details of sample preparation can be found in section 3.4 and 4.4 of this dissertation.

Optical microscopy

Details of optical microscopy can be found in section 4.4 of this dissertation.

5.4.2 Single molecule on rate and diffusion probing assay

Before the addition of labeled protein, bilayer samples were imaged to determine the impurity level. Only samples containing few (< 5) fluorescent impurities under the field of view (81µm x 81µm) were used. To start the experiment, 50 pM of Atto-RGcec (200 uL) in reaction buffer containing 1mM TCEP and 120 uM nucleotide was added to bilayer samples and the system was allowed to reach equilibrium for 5 minutes. The equilibrium was confirmed by continuously counting the number of bound mobile proteins on the surface (data now shown). Two consecutive TIRF movie streams were acquired at a frame rate of 32 Hz. The first movie was used to bleach immobile Atto-RGcec (presumably a result of protein denaturation). Only the second TIRF data was used for the on rate and diffusion analysis.

5.4.3 Protein pulse assay

This assay involves the automated stage movement (100 μm) that was incorporated into the data acquisition. To perform the measurement, 1nM Atto-RGcec (200 uL) in reaction buffer containing 1mM TCEP was injected as a pulse at 2mL/min into the bilayer samples, during which time Atto-RGcec has the chance to bind Ras on the surface. This protein pulse was directly followed by 6 mL of buffer wash at 1mL/min, allowing the removal of nonspecifically bound proteins. Both during and after the protein pulse, 10 TIRF images of Atto-RGcec were taken at multiple positions to allow the direct counting of membrane recruited Atto-RGcec.

We assume only mobile Atto-RGcec is a result of functional binding. By analyzing10 consecutive TIRF images, one can distinguish mobile and immobile proteins and hence count only mobile ones.

Single molecule corral assay and analysis

Details of this assay and analysis can be found in section 4.4 and 4.5 of this dissertation.

5.4.4 Single molecule on rate and diffusion analysis

The assay measures the binding events of labeled protein on the surface. In order to distinguish between transient, nonspecific diffusion near the surface and specific binding to the membrane, only particles lasted for at least 5 frames (155 msec) were accepted and being counted as a bound protein. A plot of accumulated counts as a function of time was constructed by summing up the number of accepted particles over the course of measurement (Fig. 5-3(A)). By fitting the slope of such plot, one can obtain the corresponding membrane on rate.

For diffusion analysis, a step-size distribution was obtained by collecting all step sizes that have the same time interval *t* (31 msec) during data acquisition. Usually, several thousands of step sizes were plotted and used for determining the diffusion coefficient. The probability density for a particle to move a distance *r* in time-interval *t* when the particle can be ascribed with a diffusion constant D (*52*):

$$\rho(r,t,D) = \frac{r}{2Dt} exp\left(-\frac{r^2}{4Dt}\right) \qquad \text{(S1)}$$

RasGRP1 samples were found to be poorly described by a single component diffusion model but was well fitted with either two- (Eq. S2) or three-component model (Eq. S3). The two-component model was found sufficient to describe the diffusion of RGcec on bilayers without Ras, whereas fitting with the three-component model was necessary for Ras functionalized samples (Fig. 5-7). In the fitting, α, α1 and α2 were treated as an independent parameter and provide the relative weight of the two or three populations.

$$\rho(r,t,D_1,D_2,\alpha) = \frac{\alpha r}{2D_1 t} exp\left(-\frac{r^2}{4D_1 t}\right) + \frac{(1-\alpha)r}{2D_2 t} exp\left(-\frac{r^2}{4D_2 t}\right) \quad \text{(S2)}$$

$$\rho(r,t,D_1,D_2,D_3,\alpha_1,\alpha_2) = \frac{\alpha_1 r}{2D_1 t} exp\left(-\frac{r^2}{4D_1 t}\right) + \frac{\alpha_2 r}{2D_2 t} exp\left(-\frac{r^2}{4D_2 t}\right) + \frac{(1-\alpha_1-\alpha_2)r}{2D_3 t} exp\left(-\frac{r^2}{4D_3 t}\right) \quad \text{(S3)}$$

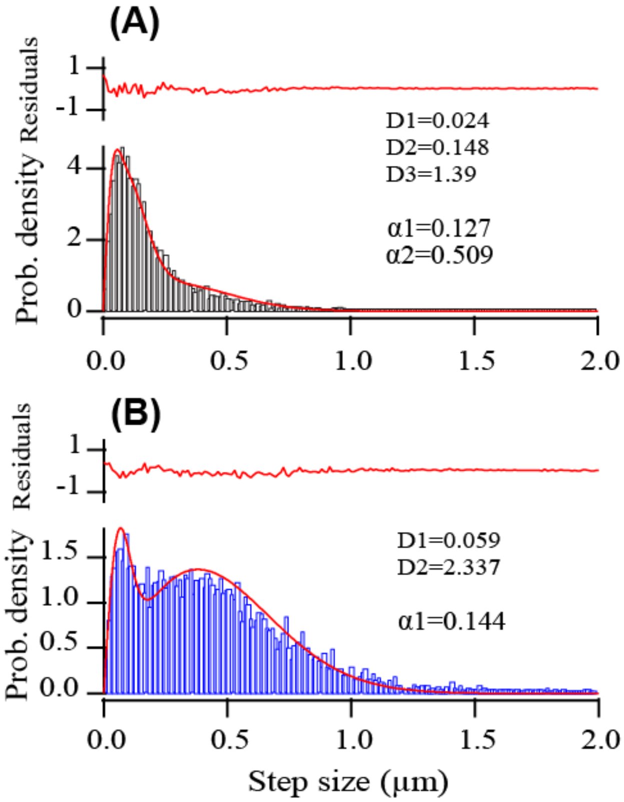

Figure 5-7. The preliminary diffusion analysis of Atto-RGcec. Based on the step-size distribution, three- or two-component diffusion models were used to describe the diffusion of Atto-RGcec on DAG bilayers (A) with and (B) without Ras functionalization, respectively. For the distribution shown here, the time interval is 31 msec and total numbers of steps is 9504 (for A) and 7443 (for B). The preliminary analysis provides the relative weight (α) and diffusion coefficient (D) of distinct diffusing species.

Bibliography

1. D. M. Engelman, Membranes are more mosaic than fluid. *Nature* **438**, 578-580 (2005).
2. C. Eggeling, C. Ringemann, R. Medda, G. Schwarzmann, K. Sandhoff, S. Polyakova, V. N. Belov, B. Hein, C. von Middendorff, A. Schonle, S. W. Hell, Direct observation of the nanoscale dynamics of membrane lipids in a living cell. *Nature* **457**, 1159-1162 (2009).
3. J. T. Groves, J. Kuriyan, Molecular mechanisms in signal transduction at the membrane. *Nature Struct. Mol. Biol.* **17**, 659-665 (2010).
4. K. Moravcevic, C. L. Oxley, M. A. Lemmon, Conditional peripheral membrane proteins: facing up to limited specificity. *Structure* **20**, 15-27 (2012).
5. M. A. Lemmon, Membrane recognition by phospholipid-binding domains. *Nature Rev. Mol. Cell Biol.* **9**, 99-111 (2008).
6. B. N. Kholodenko, J. B. Hoek, H. V. Westerhoff, Why cytoplasmic signalling proteins should be recruited to cell membranes. *Trends Cell Biol.* **10**, 173-178 (2000).
7. J. D. Scott, T. Pawson, Cell signaling in space and time: where proteins come together and when they're apart. *Science* **326**, 1220-1224 (2009).
8. K. Wennerberg, K. L. Rossman, C. J. Der, The Ras superfamily at a glance. *J. Cell Sci.* **118**, 843-846 (2005).
9. C. Lenzen, R. H. Cool, H. Prinz, J. Kuhlmann, A. Wittinghofer, Kinetic analysis by fluorescence of the interaction between Ras and the catalytic domain of the guanine nucleotide exchange factor Cdc25(Mm). *Biochemistry-Us* **37**, 7420-7430 (1998).
10. A. E. Karnoub, R. A. Weinberg, Ras oncogenes: split personalities. *Nature Rev. Mol. Cell Biol.* **9**, 517-531 (2008).
11. A. Mor, M. R. Philips, Compartmentalized Ras/MAPK signaling. *Annu. Rev. Immunol.* **24**, 771-800 (2006).
12. I. M. Ahearn, K. Haigis, D. Bar-Sagi, M. R. Philips, Regulating the regulator: post-translational modification of RAS. *Nature Rev. Mol. Cell Biol.* **13**, 39-51 (2012).
13. S. Schubbert, K. Shannon, G. Bollag, Hyperactive Ras in developmental disorders and cancer. *Nature Rev. Cancer* **7**, 295-308 (2007).

14. D. Vigil, J. Cherfils, K. L. Rossman, C. J. Der, Ras superfamily GEFs and GAPs: validated and tractable targets for cancer therapy? *Nature Rev. Cancer* **10**, 842-857 (2010).
15. J. Colicelli, Human RAS superfamily proteins and related GTPases. *Sci STKE* **2004**, RE13 (2004).
16. S. E. Neal, J. F. Eccleston, A. Hall, M. R. Webb, Kinetic analysis of the hydrolysis of GTP by p21N-ras. The basal GTPase mechanism. *J. Biol. Chem.* **263**, 19718-19722 (1988).
17. J. L. Bos, H. Rehmann, A. Wittinghofer, GEFs and GAPs: Critical elements in the control of small G proteins. *Cell* **130**, 385-385 (2007).
18. I. R. Vetter, A. Wittinghofer, The guanine nucleotide-binding switch in three dimensions. *Science* **294**, 1299-1304 (2001).
19. J. Cherfils, M. Zeghouf, Regulation of small GTPases by GEFs, GAPs, and GDIs. *Physiol Rev.* **93**, 269-309 (2013).
20. D. Stalder, H. Barelli, R. Gautier, E. Macia, C. L. Jackson, B. Antonny, Kinetic studies of the Arf activator Arno on model membranes in the presence of Arf effectors suggest control by a positive feedback loop. *J. Biol. Chem.* **286**, 3873-3883 (2011).
21. P. Chardin, S. Paris, B. Antonny, S. Robineau, S. Beraud-Dufour, C. L. Jackson, M. Chabre, A human exchange factor for ARF contains Sec7- and pleckstrin-homology domains. *Nature* **384**, 481-484 (1996).
22. S. M. Soisson, A. S. Nimnual, M. Uy, D. Bar-Sagi, J. Kuriyan, Crystal structure of the Dbl and pleckstrin homology domains from the human Son of sevenless protein. *Cell* **95**, 259-268 (1998).
23. P. A. Boriack-Sjodin, S. M. Margarit, D. Bar-Sagi, J. Kuriyan, The structural basis of the activation of Ras by Sos. *Nature* **394**, 337-343 (1998).
24. S. M. Margarit, H. Sondermann, B. E. Hall, B. Nagar, A. Hoelz, M. Pirruccello, D. Bar-Sagi, J. Kuriyan, Structural evidence for feedback activation by Ras.GTP of the Ras-specific nucleotide exchange factor SOS. *Cell* **112**, 685-695 (2003).
25. H. Sondermann, S. M. Soisson, S. Boykevisch, S. S. Yang, D. Bar-Sagi, J. Kuriyan, Structural analysis of autoinhibition in the Ras activator Son of sevenless. *Cell* **119**, 393-405 (2004).
26. J. Gureasko, W. J. Galush, S. Boykevisch, H. Sondermann, D. Bar-Sagi, J. T. Groves, J. Kuriyan, Membrane-dependent signal integration by the Ras activator Son of sevenless. *Nature Struct. Mol. Biol.* **15**, 452-461 (2008).
27. J. Gureasko, O. Kuchment, D. L. Makino, H. Sondermann, D. Bar-Sagi, J. Kuriyan, Role of the histone domain in the autoinhibition and activation of the Ras activator Son of Sevenless. *Proc. Natl. Acad. Sci. U.S.A.* **107**, 3430-3435 (2010).
28. J. Das, M. Ho, J. Zikherman, C. Govern, M. Yang, A. Weiss, A. K. Chakraborty, J. P. Roose, Digital signaling and hysteresis characterize ras activation in lymphoid cells. *Cell* **136**, 337-351 (2009).
29. G. M. Findlay, M. J. Smith, F. Lanner, M. S. Hsiung, G. D. Gish, E. Petsalaki, K. Cockburn, T. Kaneko, H. Huang, R. D. Bagshaw, T. Ketela, M. Tucholska, L.

Taylor, D. D. Bowtell, J. Moffat, M. Ikura, S. S. Li, S. S. Sidhu, J. Rossant, T. Pawson, Interaction domains of sos1/grb2 are finely tuned for cooperative control of embryonic stem cell fate. *Cell* **152**, 1008-1020 (2013).

30. J. G. Carlton, P. J. Cullen, Coincidence detection in phosphoinositide signaling. *Trends Cell Biol.* **15**, 540-547 (2005).
31. J. W. Yu, J. M. Mendrola, A. Audhya, S. Singh, D. Keleti, D. B. DeWald, D. Murray, S. D. Emr, M. A. Lemmon, Genome-wide analysis of membrane targeting by S. cerevisiae pleckstrin homology domains. *Mol. Cell* **13**, 677-688 (2004).
32. A. M. Lebensohn, M. W. Kirschner, Activation of the WAVE complex by coincident signals controls actin assembly. *Mol. Cell* **36**, 512-524 (2009).
33. A. C. Newton, Protein kinase C: poised to signal. *Am. J. Physiol. Endo. Metab.* **298**, E395-402 (2010).
34. J. C. Stone, Regulation and Function of the RasGRP Family of Ras Activators in Blood Cells. *Genes & Cancer* **2**, 320-334 (2011).
35. J. O. Ebinu, D. A. Bottorff, E. Y. W. Chan, S. L. Stang, R. J. Dunn, J. C. Stone, RasGRP, a Ras guanyl nucleotide-releasing protein with calcium- and diacylglycerol-binding motifs. *Science* **280**, 1082-1086 (1998).
36. F. Colon-Gonzalez, M. G. Kazanietz, C1 domains exposed: from diacylglycerol binding to protein-protein interactions. *Biochim. Biophys. Acta* **1761**, 827-837 (2006).
37. A. C. Newton, Protein kinase C: structure, function, and regulation. *J. Biol. Chem.* **270**, 28495-28498 (1995).
38. J. O. Ebinu, S. L. Stang, C. Teixeira, D. A. Bottorff, J. Hooton, P. M. Blumberg, M. Barry, R. C. Bleakley, H. L. Ostergaard, J. C. Stone, RasGRP links T-cell receptor signaling to Ras. *Blood* **95**, 3199-3203 (2000).
39. W.-C. Lin, C.-H. Yu, S. Triffo, J. T. Groves, in *Current Protocols in Chemical Biology*. (John Wiley & Sons, Inc., 2009), vol. 2, pp. 235-269.
40. L. K. Tamm, J. T. Groves, Supported membranes in structural biology. *J Struct Biol* **168**, 1-2 (2009).
41. J. Salafsky, J. T. Groves, S. G. Boxer, Architecture and function of membrane proteins in planar supported bilayers: A study with photosynthetic reaction centers. *Biochemistry-Us* **35**, 14773-14781 (1996).
42. P. M. Nair, K. Salaita, R. S. Petit, J. T. Groves, Using patterned supported lipid membranes to investigate the role of receptor organization in intercellular signaling. *Nature Protoc.* **6**, 523-539 (2011).
43. T. Lohmuller, L. Iversen, M. Schmidt, C. Rhodes, H. L. Tu, W. C. Lin, J. T. Groves, Single Molecule Tracking on Supported Membranes with Arrays of Optical Nanoantennas. *Nano. Lett.* **12**, 1717-1721 (2012).
44. A. D. Cox, C. J. Der, Ras history: The saga continues. *Small GTPases* **1**, 2-27 (2010).
45. M. Moertelmaier, M. Brameshuber, M. Linimeier, G. J. Schutz, H. Stockinger, Thinning out clusters while conserving stoichiometry of labeling. *App. Phys. Lett.* **87**, (2005).

46. J. Guldenhaupt, T. Rudack, P. Bachler, D. Mann, G. Triola, H. Waldmann, C. Kotting, K. Gerwert, N-Ras Forms Dimers at POPC Membranes. *Biophys. J.* **103**, 1585-1593 (2012).
47. K. Salaita, P. M. Nair, R. S. Petit, R. M. Neve, D. Das, J. W. Gray, J. T. Groves, Restriction of receptor movement alters cellular response: physical force sensing by EphA2. *Science* **327**, 1380-1385 (2010).
48. K. D. Mossman, G. Campi, J. T. Groves, M. L. Dustin, Altered TCR signaling from geometrically repatterned immunological synapses. *Science* **310**, 1191-1193 (2005).
49. H. R. Mott, J. W. Carpenter, S. L. Campbell, Structural and functional analysis of a mutant Ras protein that is insensitive to nitric oxide activation. *Biochemistry* **36**, 3640-3644 (1997).
50. S. B. Triffo, H. H. Huang, A. W. Smith, E. T. Chou, J. T. Groves, Monitoring lipid anchor organization in cell membranes by PIE-FCCS. *J. Am. Chem. Soc.* **134**, 10833-10842 (2012).
51. Y. Chen, J. D. Muller, K. M. Berland, E. Gratton, Fluorescence fluctuation spectroscopy. *Methods* **19**, 234-252 (1999).
52. A. Einstein, Über die von der molekularkinetischen Theorie der Wärme geforderte Bewegung von in ruhenden Flüssigkeiten suspendierten Teilchen. *Annalen der Physik* **17**, 549-560 (1905).
53. J. G. Zalatan, S. M. Coyle, S. Rajan, S. S. Sidhu, W. A. Lim, Conformational control of the Ste5 scaffold protein insulates against MAP kinase misactivation. *Science* **337**, 1218-1222 (2012).
54. K. E. Prehoda, J. A. Scott, R. D. Mullins, W. A. Lim, Integration of multiple signals through cooperative regulation of the N-WASP-Arp2/3 complex. *Science* **290**, 801-806 (2000).
55. M. A. Pufall, B. J. Graves, Autoinhibitory domains: modular effectors of cellular regulation. *Annu. Rev. Cell Dev. Biol.* **18**, 421-462 (2002).
56. J. E. Dueber, B. J. Yeh, K. Chak, W. A. Lim, Reprogramming control of an allosteric signaling switch through modular recombination. *Science* **301**, 1904-1908 (2003).
57. K. L. Rossman, C. J. Der, J. Sondek, GEF means go: turning on RHO GTPases with guanine nucleotide-exchange factors. *Nature Rev. Mol. Cell Biol.* **6**, 167-180 (2005).
58. T. S. Freedman, H. Sondermann, G. D. Friedland, T. Kortemme, D. Bar-Sagi, S. Marqusee, J. Kuriyan, A Ras-induced conformational switch in the Ras activator Son of sevenless. *Proc. Natl. Acad. Sci. U.S.A.* **103**, 16692-16697 (2006).
59. M. Tartaglia, L. A. Pennacchio, C. Zhao, K. K. Yadav, V. Fodale, A. Sarkozy, B. Pandit, K. Oishi, S. Martinelli, W. Schackwitz, A. Ustaszewska, J. Martin, J. Bristow, C. Carta, F. Lepri, C. Neri, I. Vasta, K. Gibson, C. J. Curry, J. P. Siguero, M. C. Digilio, G. Zampino, B. Dallapiccola, D. Bar-Sagi, B. D. Gelb, Gain-of-function SOS1 mutations cause a distinctive form of Noonan syndrome. *Nature Genet.* **39**, 75-79 (2007).
60. A. E. Roberts, T. Araki, K. D. Swanson, K. T. Montgomery, T. A. Schiripo, V. A. Joshi, L. Li, Y. Yassin, A. M. Tamburino, B. G. Neel, R. S. Kucherlapati, Germline

gain-of-function mutations in SOS1 cause Noonan syndrome. *Nature Genet.* **39**, 70-74 (2007).

61. S. Boykevisch, C. Zhao, H. Sondermann, P. Philippidou, S. Halegoua, J. Kuriyan, D. Bar-Sagi, Regulation of ras signaling dynamics by Sos-mediated positive feedback. *Curr. Biol.* **16**, 2173-2179 (2006).
62. A. Prasad, J. Zikherman, J. Das, J. P. Roose, A. Weiss, A. K. Chakraborty, Origin of the sharp boundary that discriminates positive and negative selection of thymocytes. *Proc. Natl. Acad. Sci. U.S.A.* **106**, 528-533 (2009).
63. J. P. Roose, M. Mollenauer, M. Ho, T. Kurosaki, A. Weiss, Unusual interplay of two types of Ras activators, RasGRP and SOS, establishes sensitive and robust Ras activation in lymphocytes. *Mol. Cell. Biol.* **27**, 2732-2745 (2007).
64. K. K. Yadav, D. Bar-Sagi, Allosteric gating of Son of sevenless activity by the histone domain. *Proc. Natl. Acad. Sci. U.S.A.* **107**, 3436-3440 (2010).
65. D. D. Boehr, R. Nussinov, P. E. Wright, The role of dynamic conformational ensembles in biomolecular recognition. *Nature Chem. Biol.* **5**, 789-796 (2009).
66. S. R. Tzeng, C. G. Kalodimos, Dynamic activation of an allosteric regulatory protein. *Nature* **462**, 368-372 (2009).
67. S. R. Tzeng, C. G. Kalodimos, Protein activity regulation by conformational entropy. *Nature* **488**, 236-240 (2012).
68. K. Henzler-Wildman, D. Kern, Dynamic personalities of proteins. *Nature* **450**, 964-972 (2007).
69. K. A. Henzler-Wildman, M. Lei, V. Thai, S. J. Kerns, M. Karplus, D. Kern, A hierarchy of timescales in protein dynamics is linked to enzyme catalysis. *Nature* **450**, 913-916 (2007).
70. W. Min, G. Luo, B. J. Cherayil, S. C. Kou, X. S. Xie, Observation of a power-law memory kernel for fluctuations within a single protein molecule. *Phys. Rev. Lett.* **94**, 198302 (2005).
71. R. G. Smock, L. M. Gierasch, Sending signals dynamically. *Science* **324**, 198-203 (2009).
72. P. Li, I. R. Martins, G. K. Amarasinghe, M. K. Rosen, Internal dynamics control activation and activity of the autoinhibited Vav DH domain. *Nature Struct. Mol. Biol.* **15**, 613-618 (2008).
73. T. S. Freedman, H. Sondermann, O. Kuchment, G. D. Friedland, T. Kortemme, J. Kuriyan, Differences in flexibility underlie functional differences in the Ras activators son of sevenless and Ras guanine nucleotide releasing factor 1. *Structure* **17**, 41-53 (2009).
74. H. P. Lu, L. Xun, X. S. Xie, Single-molecule enzymatic dynamics. *Science* **282**, 1877-1882 (1998).
75. B. P. English, W. Min, A. M. van Oijen, K. T. Lee, G. Luo, H. Sun, B. J. Cherayil, S. C. Kou, X. S. Xie, Ever-fluctuating single enzyme molecules: Michaelis-Menten equation revisited. *Nature Chem. Biol.* **2**, 87-94 (2006).

76. M. K. Prakash, R. A. Marcus, An interpretation of fluctuations in enzyme catalysis rate, spectral diffusion, and radiative component of lifetimes in terms of electric field fluctuations. *Proc. Natl. Acad. Sci. U.S.A.* **104**, 15982-15987 (2007).
77. C. Frieden, Slow transitions and hysteretic behavior in enzymes. *Annu. Rev. Biochem.* **48**, 471-489 (1979).
78. E. Leikina, C. Ramos, I. Markovic, J. Zimmerberg, L. V. Chernomordik, Reversible stages of the low-pH-triggered conformational change in influenza virus hemagglutinin. *EMBO J.* **21**, 5701-5710 (2002).
79. A. Behzadi, R. Hatleskog, P. Ruoff, Hysteretic enzyme adaptation to environmental pH: change in storage pH of alkaline phosphatase leads to a pH-optimum in the opposite direction to the applied change. *Biophys. Chem.* **77**, 99-109 (1999).
80. B. H. Toyama, M. W. Hetzer, Protein homeostasis: live long, won't prosper. *Nature Rev. Mol. Cell Biol.* **14**, 55-61 (2013).
81. Z. Wu, J. Xing, Functional roles of slow enzyme conformational changes in network dynamics. *Biophys. J.* **103**, 1052-1059 (2012).
82. S. R. Sprang, Conformational display: a role for switch polymorphism in the superfamily of regulatory GTPases. *Science's STKE : signal transduction knowledge environment* **2000**, pe1 (2000).
83. S. Kapoor, G. Triola, I. R. Vetter, M. Erlkamp, H. Waldmann, R. Winter, Revealing conformational substates of lipidated N-Ras protein by pressure modulation. *Proc. Natl. Acad. Sci. U.S.A.* **109**, 460-465 (2012).
84. F. Raimondi, G. Portella, M. Orozco, F. Fanelli, Nucleotide binding switches the information flow in ras GTPases. *PLoS Comput. Biol.* **7**, e1001098 (2011).
85. M. Spoerner, A. Nuehs, C. Herrmann, G. Steiner, H. R. Kalbitzer, Slow conformational dynamics of the guanine nucleotide-binding protein Ras complexed with the GTP analogue GTPgammaS. *FEBS J.* **274**, 1419-1433 (2007).
86. W. J. Albery, J. R. Knowles, Evolution of enzyme function and the development of catalytic efficiency. *Biochemistry-Us* **15**, 5631-5640 (1976).
87. M. S. Samoilov, G. Price, A. P. Arkin, From fluctuations to phenotypes: the physiology of noise. *Sci STKE* **2006**, re17 (2006).
88. A. Eldar, M. B. Elowitz, Functional roles for noise in genetic circuits. *Nature* **467**, 167-173 (2010).
89. Y. Wakamoto, N. Dhar, R. Chait, K. Schneider, F. Signorino-Gelo, S. Leibler, J. D. McKinney, Dynamic persistence of antibiotic-stressed mycobacteria. *Science* **339**, 91-95 (2013).
90. H. Qian, Cooperativity in cellular biochemical processes: noise-enhanced sensitivity, fluctuating enzyme, bistability with nonlinear feedback, and other mechanisms for sigmoidal responses. *Annu. Rev. Biophys.* **41**, 179-204 (2012).
91. R. Losick, C. Desplan, Stochasticity and cell fate. *Science* **320**, 65-68 (2008).
92. P. J. Choi, L. Cai, K. Frieda, X. S. Xie, A stochastic single-molecule event triggers phenotype switching of a bacterial cell. *Science* **322**, 442-446 (2008).
93. H. Sondermann, B. Nagar, D. Bar-Sagi, J. Kuriyan, Computational docking and solution x-ray scattering predict a membrane-interacting role for the histone domain

of the Ras activator son of sevenless. *Proc. Natl. Acad. Sci. U.S.A.* **102**, 16632-16637 (2005).

94. S. C. Kou, B. J. Cherayil, W. Min, B. P. English, X. S. Xie, Single-molecule Michaelis-Menten equations. *J. Phys. Chem. B* **109**, 19068-19081 (2005).
95. D. L. Ensign, V. S. Pande, Bayesian detection of intensity changes in single molecule and molecular dynamics trajectories. *J. Phys. Chem. B* **114**, 280-292 (2010).
96. D. T. Gillespie, A general method for numerically simulating the stochastic time evolution of coupled chemical reactions. *J. Comput. Phys.* **22**, 403-434 (1976).
97. L. H. Chao, M. M. Stratton, I. H. Lee, O. S. Rosenberg, J. Levitz, D. J. Mandell, T. Kortemme, J. T. Groves, H. Schulman, J. Kuriyan, A mechanism for tunable autoinhibition in the structure of a human Ca2+/calmodulin- dependent kinase II holoenzyme. *Cell* **146**, 732-745 (2011).
98. A. D. Nancy, L. S. Stacey, A. B. Drell, O. E. Julius, D. Peter, L. O. Hanne, C. S. James, RasGRP is essential for mouse thymocyte differentiation and TCR signaling. *Nature Immunol.* **1**, 317-321 (2000).
99. R. L. Kortum, A. K. Rouquette-Jazdanian, L. E. Samelson, Ras and extracellular signal-regulated kinase signaling in thymocytes and T cells. *Trends Immunol.* (2013).
100. N. C. Strynadka, M. N. James, Crystal structures of the helix-loop-helix calcium-binding proteins. *Annual. Rev. Biochem.* **58**, 951-998 (1989).
101. C. E. Tognon, H. E. Kirk, L. A. Passmore, I. P. Whitehead, C. J. Der, R. J. Kay, Regulation of RasGRP via a phorbol ester-responsive C1 domain. *Mol. Cell. Biol.* **18**, 6995-7008 (1998).
102. J. P. Roose, M. Mollenauer, V. A. Gupta, J. Stone, A. Weiss, A diacylglycerol-protein kinase C-RasGRP1 pathway directs Ras activation upon antigen receptor stimulation of T cells. *Mol. Cell. Biol.* **25**, 4426-4441 (2005).
103. P. S. Lorenzo, M. Beheshti, G. R. Pettit, J. C. Stone, P. M. Blumberg, The guanine nucleotide exchange factor RasGRP is a high-affinity target for diacylglycerol and phorbol esters. *Mol. Pharmacol.* **57**, 840-846 (2000).
104. G. Tazmini, N. Beaulieu, A. Woo, B. Zahedi, R. E. Goulding, R. J. Kay, Membrane localization of RasGRP1 is controlled by an EF-hand, and by the GEF domain. *Biochim. Biophys. Acta Mol. Cell Res.* **1793**, 447-461 (2009).
105. N. Beaulieu, B. Zahedi, R. E. Goulding, G. Tazmini, K. V. Anthony, S. L. Omeis, D. R. de Jong, R. J. Kay, Regulation of RasGRP1 by B Cell Antigen Receptor Requires Cooperativity between Three Domains Controlling Translocation to the Plasma Membrane. *Mol. Biol. Cell* **18**, 3156-3168 (2007).
106. D. M. Fuller, M. Zhu, X. Song, C. W. Ou-Yang, S. A. Sullivan, J. C. Stone, W. Zhang, Regulation of RasGRP1 function in T cell development and activation by its unique tail domain. *Plos One* **7**, e38796 (2012).
107. L. O. Murphy, J. P. MacKeigan, J. Blenis, A network of immediate early gene products propagates subtle differences in mitogen-activated protein kinase signal amplitude and duration. *Mol. Cell. Biol.* **24**, 144-153 (2004).

108. Jeremy E. Purvis, G. Lahav, Encoding and Decoding Cellular Information through Signaling Dynamics. *Cell* **152**, 945-956 (2013).

Appendix 1. Assay Details

A-1. Hybrid pulse chase assay

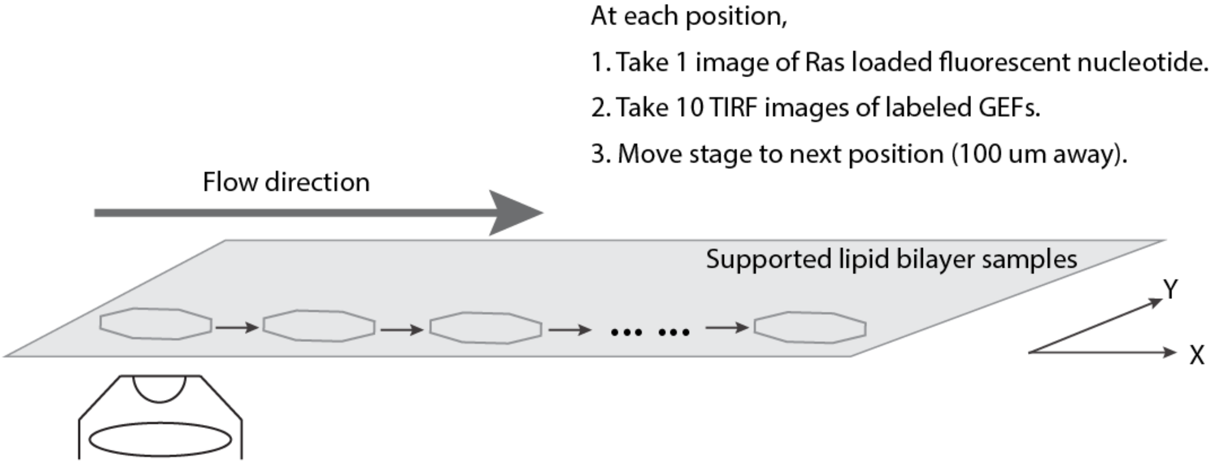

Figure A-1. An illustration of hybrid pulse-chase assay. The kinetics of GEF-catalyzed nucleotide exchange reaction can be followed as the objective moves along the supported bilayer surface during the reaction.

The purpose of hybrid pulse-chase assay is to study the kinetics of GEF-catalyzed nucleotide exchange reaction on the supported bilayer system. The assay aims to probe how enzyme catalyzes its substrates on the surface. The whole process, in the case of membrane associated protein-protein interactions, involves initial membrane localization, binding and catalyzing substrates and finally the unbinding of the protein from the membrane. To perform hybrid pulse-chase assay,

- Labeled and unlabeled proteins (such as RGcec constructs used in chapter 5 of this dissertation) are firstly mixed. The ratio between the two proteins is determined based on detailed experimental conditions (typically labeled/unlabeled = 1/20). A general guideline is that total protein concentration (labeled + unlabeled) should be high enough (in the case of RGcec, it is 100 nM) to provide well-resolved and clear activity traces. On the other hand, concentration of the labeled protein should be relatively low to allow the visualization and counting of the bound protein on the membrane.
- The protein mixture is then injected as a pulse into the reaction chamber.

  - Considerations: flow rate is determined experimentally. Typical flow rates used in this dissertation range from 1 – 2.5 mL/min.
- During protein pulse, 10 consecutive TIRF images of the labeled protein are taken to record the number of bound protein on the bilayer surface. This data is analyzed and later used to calculate the recruitment tendency across different experimental conditions.
- The exchange reaction is initiated when unlabeled nucleotide (such as GDP or GTP) is injected into the system as a continuous flow at 0.2-1 mL/min flow rate.

- During the exchange reaction, a journal in Metamorph is recorded and utilized to allow data acquisition at pre-defined position on the supported bilayer surface (Fig. A-1). Specifically, 1 epi-image of fluorescent nucleotide loaded Ras and 10 TIRF images of labeled protein (such as RGcec in chapter 4) are taken at each position. Following the intensity trace from Ras channel allows one to obtain the activity due to GEF-catalyzed exchange reaction, whereas 10 TIRF images allow direct measurement of the number of bound protein. We assume only mobile protein is the result of functional binding and can contribute to turnovers. By analyzing10 consecutive TIRF images, one can distinguish mobile and immobile proteins and hence count only mobile ones for later analysis. The details of analysis for hybrid pulse-chase data can be found in section 5.4 in this dissertation.

A-2. Single molecule on rate, diffusion and residence time probing assay

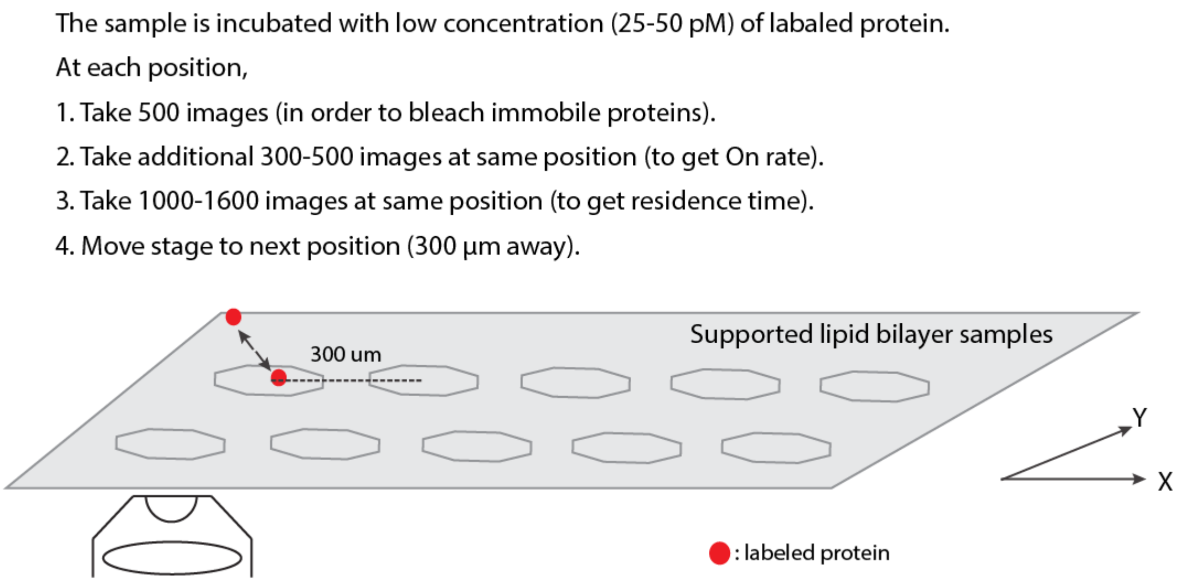

The sample is incubated with low concentration (25-50 pM) of labaled protein.

At each position,

1. Take 500 images (in order to bleach immobile proteins).
2. Take additional 300-500 images at same position (to get On rate).
3. Take 1000-1600 images at same position (to get residence time).
4. Move stage to next position (300 µm away).

Figure A-2. An illustration of single molecule on-rate measurement. By measuring the number of proteins on the surface as a function of time during protein incubation, one can probe the on-rate, diffusion and residence time of proteins of interest on the membrane.

This assay provides direct measurement on how protein binds to the supported membrane. It is useful if one wants to study the effect of lipids and/or proteins in localizing proteins to the surface. To perform this measurement,

- Prepare the supported membrane with proteins (or lipids) of interest and confirm the two dimensional fluidity of the sample by performing FRAP or FCS measurements.

  - Considerations: Depending on the type of experiment, usually various standard epi-fluorescence images will be acquired in order to obtain the calibration curve and/or the surface density of the lipids/proteins.

- Prepare labeled protein at relative low concentration (in the case of RGcec, it is 50 pM). It is important to optimize the concentration of labeled protein for this step.

  - Considerations: Too high concentration might make the following analysis very challenging.

- Flow in labeled protein and allow the system to reach binding equilibrium. The equilibrium can be measured by direct imaging of the number of bound protein as a function of time. In the case of SOS and RGcec, the system reaches equilibrium after 5 minutes.

- At each position, take 2 consecutive TIRF stream (500 frames) of labeled protein at fast frame rate (~ 30-40 Hz). The first TIRF movie is used to bleach immobile proteins and the second TIRF data is used for on-rate and diffusion analysis. The details of analysis for hybrid pulse-chase data can be found in section 5.4 in this dissertation.
- (Optional) If one also wants to probe the residence time, take an additional TIRF stream at slower frame rate (~ 3Hz) with lower laser power at the “pre-bleached” spot. The less-frequent imaging condition reduces bleaching and allows longer tracking and residence time measurements.

  - Considerations: In order to resolve single molecule in the analysis, one needs to find a good balance between laser power, exposure time and frame rate.